Modelling CO_2 hydrogenation reaction on Pt functionalized UiO-67 Metal-Organic Frameworks

Sri Harsha Pulumati

Faculty of Industrial Engineering, Mechanical Engineering and Computer Science
University of Iceland
2024

Modelling CO_2 hydrogenation reaction on Pt functionalized UiO-67 Metal-Organic Frameworks

Sri Harsha Pulumati

Dissertation submitted in partial fulfilment of a
Philosophiae Doctor degree in Chemical Engineering

Advisor
Prof. Egill Skúlason

PhD Committee
Prof. Egill Skúlason
Prof. Hannes Jónsson
Dr. Ainara Nova

Opponents
Prof. Mårten Ahlquist
Dr. Manuel A. Ortuño

Faculty of Industrial Engineering, Mechanical Engineering
and Computer Sciences
University of Iceland
Reykjavik, February 2024

Modelling CO_2 hydrogenation reaction on Pt functionalized UiO-67 Metal-Organic Frameworks.
Dissertation submitted in partial fulfilment of a *Philosophiae Doctor* degree in Chemical Engineering.

Faculty of Industrial Engineering, Mechanical Engineering and Computer Sciences
School of Engineering and Natural Sciences
University of Iceland
Tæknigarður, Dunhaga 5
107, Reykjavik
Iceland

Bibliographic information:
Sri Harsha Pulumati, 2023, *Modelling CO_2 hydrogenation reaction on Pt functionalized UiO-67 Metal-Organic Frameworks*, PhD dissertation, Faculty of Industrial Engineering, Mechanical Engineering and Computer Sciences,
University of Iceland.

ISBN: 978-9935-9768-0-2

Author ORCID: 0009-0001-6287-7620

Printing: Háskólaprent ehf, Fálkagata 2, 107 Reykjavík

Reykjavik, Iceland, February2024

This dissertation is dedicated to
my family and friends.

Acknowledgements

My doctoral journey, set against the awe-inspiring backdrop of beautiful Northern Lights, majestic glaciers, geysers, and the warm Icelandic community, has been a transformative experience. While writing this dissertation, I feel profound gratitude for the numerous opportunities I was given, and I will forever cherish my time as a doctoral candidate. Firstly, I would like to express my most profound appreciation to my advisors and PhD committee – Prof. Egill Skúlason and Prof. Hannes Jónsson from the University of Iceland and Dr. Ainara Nova from the University of Oslo. Their relentless guidance, generous knowledge-sharing, and rigorous critiques have been integral in my academic growth and the completion of this dissertation.

Heartfelt thanks are owed to Prof. Unni Olsbye, Dag Kristian Sannes, Dr. Torstein Fjermestad and Dr. Emil Sebastian Gutterød from the University of Oslo for their excellent collaboration. Their insightful discussions during my many enriching research visits to Oslo have broadened my horizons and deepened my comprehension of our mutual field of study.

To my beloved wife, Mounika, I am indebted with love, profound gratitude and admiration. Her unwavering support and understanding have been my bedrock throughout this academic pursuit. I sincerely thank my family for their consistent love, encouragement, and steadfast belief in me. Special mention goes to my brother, Nithin, who is preparing for his doctoral defence; my best wishes are with you. I also sincerely appreciate the 'Theochem group' at the University of Iceland, past and present members alike. Their insightful discussions, unwavering friendship, and support have made my tenure as a doctoral candidate both a joyous and enlightening experience. Finally, my sincerest thanks also go to NordCO2 and the Icelandic Research Fund for their financial backing, which was pivotal in facilitating my research and studies.

This dissertation is not only the product of my efforts but is emblematic of the cumulative support and contribution of all involved in this journey. The experiences, friendships, and opportunities afforded me during these doctoral studies are priceless, and I would willingly embark on this journey again. I wish to extend a resounding thank you to everyone who has been part of my academic expedition. Your support, guidance, and companionship have immeasurably enriched my experience. This journey transcends an academic endeavour, representing personal growth and the forging of enduring relationships.

Thank you once again!

Sri Harsha Pulumati.

Abstract

Converting CO_2 into value-added products via hydrogenation is of interest due to its potential to reduce and reuse excess atmospheric CO_2 and deal with global warming. Metal-organic frameworks (MOFs) are of great interest in this conversion process due to their appealing properties, such as high specific surface area, porosity, and a tailorable structure and function. Platinum functionalized Zr-based UiO-67 MOFs are one such MOF that demonstrate high selectivity towards methanol formation in CO_2 reduction reactions (CO2RR), outperforming other well-known metal-support catalysts. However, the CO2RR mechanisms in this catalytic system remain unclear and have been a topic of ongoing exploration. This dissertation investigates the catalytic properties and proposes mechanisms of CO_2 hydrogenation on UiO-67 MOFs embedded with Platinum nanoparticles.

In the first part of this study, density functional theory (DFT) calculations and micro-kinetic model were used along with experimental collaboration at the University in Oslo to investigate the role of missing linker defects on the Zr-nodes of UiO-67 MOF in the CO_2 hydrogenation reaction. We found that increased linker defects on the Zr-node also increase methanol and methane formation rates. We also explored the influence of H_2O on the CO_2 hydrogenation reaction, where we found that dehydrated Zr-nodes show higher methanol and methane formation rates. Interestingly, water promotes methanol desorption and does not change the steady-state reaction rate but significantly inhibits methane formation. This finding suggests that water can increase the reaction selectivity to methanol. These discoveries provide a new perspective on the dynamic role of the Zr-node and the influence of water on the reaction. It was also shown that methanol is formed at the interface between the Pt NPs and defect Zr nodes via formate species attached to the Zr nodes, which is a novel finding and understanding of the mechanistic separation between the formation of methanol and the formation of co-products of CO gas and methane became necessary. These results were published in the Journal of the American Chemical Society in 2020.

In the second part of this study, we employ DFT calculations to elucidate the CO2RR mechanism where free energy barriers were calculated between the most important intermediates from CO_2 gas to all the products: methanol, methane, and CO gas. We used five different atomistic models in order to understand the activity of individual parts of the whole system. This showed that unique and different combinations of the Zr-clusters and the Pt NP interfaces are necessary for a selective production of CO and methane on one hand and for methanol on the other hand. Our findings, supported by experiments done at the University in Oslo, suggest that the synergistic interaction resulting at the interface between Zr-clusters and Pt nanoparticle´s edges play a crucial role in the reduction reaction to methanol but not to methane nor CO gas, which rather take place at the interface of Zr-clusters and flat (111) surfaces of the Pt NPs. Furthermore, it highlights the significance of understanding both individual components of the catalytic system and their interfaces in enhancing catalytic activity. The results show that smaller Pt NPs form more methanol, whereas larger Pt NPs form more methane and CO gas. Finally, we hope this research will have potential implications for developing more efficient and selective catalysts for CO_2 hydrogenation to methanol. These results were published in ACS Catalysis in 2024.

Útdráttur

Að breyta CO_2 í verðmæt efni með afoxun er áhugavert viðfangsefni þar sem hægt er að endnýta CO_2 og lækka þar af leiðandi magn þess í andrúmslofti og leggja lið við að minnka loftlagsvánna. Stoðgrindir byggðar upp með málmlífrænum efnum (MOFs) eru áhugaverð að skoða í þessu samhengi vegna eiginleika þeirra svo sem hátt yfirborðsflatarmál sem og að hægt er að hanna byggingu þeirra og virkni á margvíslegan hátt. Platínu nanóagnir í zirkóníum UiO-67 MOFs er eitt slíkt kerfi sem hefur sýnt að hefur háa nýtni og stöðugleika til að mynda metanól í CO_2 afoxunarhvarfinu (CO2RR) í mun meira magni en aðrir efnahvatar svo sem Pt nanóagnir á flötum yfirborðum. Hins vegar hefur hvarfgangurinn verið óljós hingað til en upp á síðkasti verið kannaður með ýmsum aðferðum. Þessi doktorsritgerð rannsakar hvarfgang CO_2 afoxunar í UiO-67 MOFs sem innihalda Pt nanóagnir.

Í fyrri hluta þessarar rannsóknar voru þéttnifellafræði (DFT) reikningar notaðir og hraðafræðilegt líkan þróað í samvinnu við tilraunahóp í Háskólanum í Osló til að rannsaka hlutverk veilna þar sem lífrænn tengihópur vantaði á Zr-nóðuna í UiO-67 MOF kerfinu fyrir afoxun CO_2 hvarfsins. Við fundum út að þegar þessum veilum er fjölgað eykst bæði hraði metanóls og metans. Við rannsökuðum einnig áhrif vatns fyrir CO2RR, þar sem við fundum að þurari Zr-nóður leiða til hærri hraða á bæði myndun metanóls og metans . Athyglisvert þykir að vatn eykur frásog metanóls en breytir ekki jafnvægisástandshraðanum en kemur í veg fyrir myndun metans. Þessi niðurstaða sýnir að vatn getur aukið nýtni metanólsmyndunar. Þessar uppgötvanir gefa nýja sýn á hreyfifræðilegt hlutverk Zr-nóða og áhrif vatns á hvarfið. Einnig sýndum við fram á að metanól er myndað á skilfleti milli Pt nanóagna og Zr-nóðu með veilu í gegnum milliefnið OCHO (formate) bundið við Zr-nóðu sem er ný vitneskja. Skilningur á þessum hvarfgangi og aðskilnaði á hvarfleiðum í átt að metanóli og hliðarhvarfa í átt að CO og metans var nauðsynlegur. Þessar niðurstöður voru birtar í tímaritinu Journal of the American Chemical Society árið 2020.

Í seinni hluta rannsóknarinnar notuðum við einnig DFT reikninga til að skilja til hlýtar CO2RR hvarfganginn þar sem virkjunarhólar voru reiknaðir á milli helstu milliefna frá CO_2 gasi í öll myndefnin; metanól, metan og CO gas. Hér notuðum við fimm mismunandi atómlíkön til að skilja virkni hinna ýmsu staða í heildarkerfinu. Þar sýndum við að sérstök og mismunandi samskeyti milli Zr-klasans og Pt agnarinnar eru nauðsynleg fyrir sértæka myndun á CO gasi og metani annars vegar og fyrir metanól hins vegar. Niðurstöður okkar, sannreyndar með tilraunum í samstarfi við Háskólann í Osló, sýna að samverkandi samspil milli Zr-klasans og sérstakra veilna (brúnir/þrep/jaðrar/kantar) á Pt ögninni hefur lykiláhrif á afoxunarhvarfið og myndun á metanóli en ekki metans né CO gass sem á sér stað á skilfleti milli Zr-klasanna og flatra (111) yfirborða Pt nanóagnanna. Þar að auki sýnir þessi rannsókn hversu mikilvægt er að skilja alla mismunandi hluta kerfisins eina og sér og til hlýtar sem og skilfletina á milli þessara hluta heildar kerfisins til að hægt sé að auka hvatavirknina. Niðurstöðurnar benda til að minni Pt agnir mynda meira metanól en stærri Pt agnir mynda metan og CO gas frekar. Að lokum vonum við að þessi rannsókn megi leiða til að hægt sé að hanna betri og virkari efnahvata fyrir afoxun CO_2 í metanól. Þessar niðurstöður voru birtar í tímaritinu ACS Catalysis árið 2024.

Preface

This thesis is submitted in candidacy for a Ph.D. degree from the University of Iceland. The work was conducted between December 2018 and December 2023 at the Faculty of Industrial Engineering, Mechanical Engineering, and Computer Sciences, supervised by Prof. Egill Skúlason.

Icelandic Research Fund (Grants no. 196437-051 and 207283-051), the Research Fund of the University of Iceland, and "Nordic Consortium for CO_2 Conversion" NordForsk project No. 85378 financially supported the work.

Sri Harsha Pulumati

February2024

Table of Contents

List of Figures

List of Articles

Article I:

Emil Sebastian Gutterød, Sri Harsha Pulumati, Gurpreet Kaur, Andrea Lazzarini, Bjørn Gading Solemsli, Anette Eleonora Gunnæs, Christian Ahoba-Sam, Maria Evangelou Kalyva, Johnny Andreas Sannes, Stian Svelle, Egill Skúlason, Ainara Nova, Unni Olsbye.

"Influence of defects and H2O on the hydrogenation of CO2 to methanol over Pt nanoparticles in UiO-67 metal–organic framework."

Journal of the American Chemical Society 142, no. 40 (2020): 17105-17118.

Article II:

Sri Harsha Pulumati, Dag Kristian Sannes, Christia R.Jabbour, Laurens D.B. Mandemaker, Bert M. Weckhuysen, Unni Olsbye, Ainara Nova, and Egill Skúlason.

"Mechanistic insights for Hydrogenation of CO2 to Methanol, Methane and CO over Pt Nanoparticles in UiO-67 Metal-Organic Frameworks."

ACS Catalysis 14 (2023): 382-394.

Abbreviations

B3LYP	Becke, 3-parameter, Lee–Yang–Parr
BDC	Benzene dicarboxylic acid
BECCS	Bioenergy with carbon capture and storage
BPDC	Biphenyl dicarboxylate
BSSE	Basis set superposition error
CC	Coupled Cluster
CCS	Carbon capture and storage
CGF	Contracted Gaussian functions
CH3OH	Methanol
CH4	Methane
CI	Configuration interaction
CO	Carbon monoxide
CO_2	Carbon dioxide
CO_2RR	Carbon dioxide reduction reaction
DAC	Direct air capture
DFT	Density functional theory
EBFC	Enzymatic biofuel cell
ECR	Electrochemical CO2 reduction
FFT	Fast Fourier Transform
GGA	Generalized Gradient Approximation
GPW	Gaussian and Plane Wave
GTH	Goedecker-Tetter-Hutter
GTO	Gaussian-type orbitals
HER	Hydrogen Evolution Reaction
HF	Hatree Fock
IR	Infrared
KS	Kohn-Sham
LDA	Local Density Approximation
MEP	Minimum energy path

MKM	Micro Kenetik model
MNP	Metal nano particle
MOF	Metal-organic framework
NEB	Nudged elastic band
NP	Nanoparticle
OMS	Open metal sites
PBE	Perdew-Burke-Eernzerhof
PSE	Post-Synthetic Exchange
RDS	Rate determining step
RWGS	Reverse water gas shift
STO	Slater-type orbitals
TPDC	Terphenyl-4,4'-dicarboxylate

Thesis Outline

This study examines the properties and potential applications of Metal-Organic Frameworks (MOFs), particularly emphasizing their role in CO_2 conversion and explores the mechanism for CO_2 reduction reaction (CO_2RR) on Pt-encapsulated UiO-67 MOFs towards CO, Methanol and Methane, a topic of significant importance as a potential solution to global warming and its mitigation. The thesis starts with a discussion on global warming, where I briefly introduce the science behind global warming, exploring the role of greenhouse gases, mainly CO_2, in the warming of the planet, followed by an exploration of CO_2 conversion methods, which are presented as a potential solution to the problem of increasing atmospheric CO_2 levels.

The discussion then shifts to MOFs, a class of compounds consisting of metal ions or clusters coordinated with organic ligands to form one-, two-, or three-dimensional structures. The unique properties of MOFs, including their high porosity and tuneable chemical functionality, are explored in detail. The diverse applications of MOFs are then discussed, including their use in gas storage, water purification, chemical sensing, carbon capture and catalysis. After this, the UiO family of MOFs is introduced, the thesis's main focus. The unique properties of these MOFs, including their high stability and exceptional porosity, are discussed in detail. The potential applications of Pt-encapsulated UiO-67 MOFs in CO_2 conversion are then explored, providing a comprehensive understanding of their potential role in reducing CO_2 from the atmosphere by mitigating global warming.

The challenges faced in identifying the mechanism for the reduction reaction are then discussed, highlighting the need for computational calculations in catalyst design. This sets the stage for a detailed exploration of the study's theoretical background, including Density Functional Theory (DFT), starting from the Schrödinger equation and the Born-Oppenheimer approximation. The principles and applications of Hartree-Fock theory are then discussed, followed by an exploration of exchange-correlation functional and basis sets like Gaussian and plane wave pseudopotentials. The Gaussian and Plane Wave (GPW) method and the Nudged Elastic Band (NEB) methods used in this thesis are also introduced at this stage, providing an understanding of the computational tools used in the study. Finally, the thesis concludes with an overview of the articles published as part of this thesis work. First, the abstracts of these articles are presented, followed by the full text of the articles themselves and their Supporting Information (SI).

In this thesis, I aim to answer two primary objectives and a few research questions that provide valuable insights into the CO_2RR on Pt-encapsulated UiO-67 MOFs.

Research objectives:

1. Find the mechanism for CO_2 hydrogenation over UiO-67-Pt and reveal why the mechanism for methanol formation is distinct from CO and methane production.

2. Find the rate-limiting step for methane, methanol, and CO formation.

Research questions:

1. What is the correlation between the number of node defects and methanol and methane formation rate?

2. Why the CO formation rate is not dependent on the defect density?

3. Why does water co-feed promote the desorption of methanol and inhibit methane formation?

4. What is the role of dehydrated and pre-hydrated Zr-nodes in methanol and methane formation rates?

5. What is the reason for the prominent formate signal and CO signals?

1 Introduction

1.1 Global warming and its causes

Global warming is a phenomenon marked by a gradual increase in the Earth's average temperature due to an enhanced greenhouse effect, and it is primarily attributed to human activities. This effect is caused by greenhouse gasses that trap excess heat in the Earth's atmosphere, like glass retaining heat in a greenhouse. It is primarily driven by releasing certain gases into the atmosphere, such as carbon dioxide (CO_2) and methane (CH_4), which trap heat from the Sun.

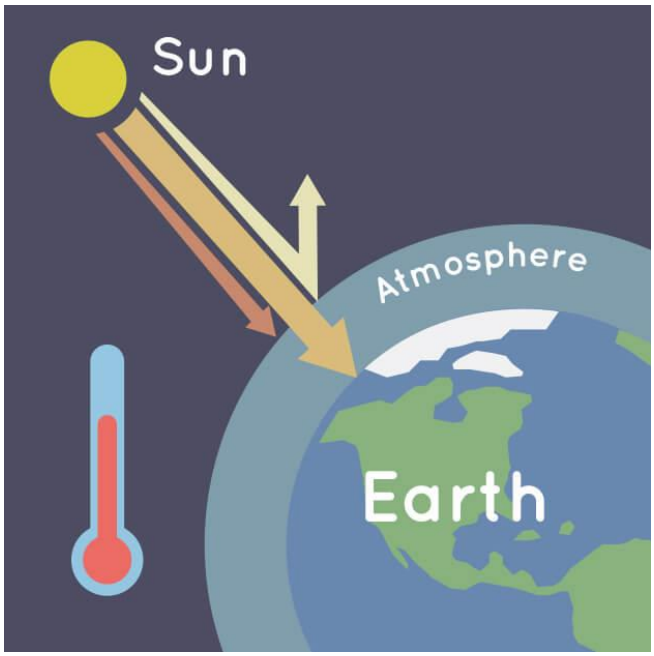

Figure 1 Global warming schematic shows Earth's atmosphere traps some of the Sun's heat, increasing global temperature. (Credit: NASA/JPL-Caltech)

While certain amounts of greenhouse gases are naturally occurring and necessary for creating a habitable climate on Earth, human activities such as burning fossil fuels, deforestation, and other intensive industrial processes have increased the concentration of these greenhouse gases in our atmosphere in recent years. This increase intensifies the greenhouse effect, leading to more heat being retained and causing Earth's average temperature to rise, resulting in climate change.

Climate change is a significant concern for life on our planet, as the atmospheric concentration of greenhouse gases has risen continuously over the last century, with CO_2 being one of the most significant contributors. CO_2 is released into the atmosphere when fossil fuels such as coal, oil, and natural gas are burned. The concentration of atmospheric CO_2 has increased from roughly ~275 ppm to ~415 ppm since 1750[2], and the primary reason for this is human activity. Without immediate action, CO_2 emissions will continue to rise as the world economy grows, with electricity generation being a major source of CO_2 produced.

The current global power consumption is around 160000 TWh, projected to double in the next decade and potentially triple by the end of the century.[3,4] Most of our energy demand is satisfied by burning fossil fuels, leading to the generation of CO_2 as the primary greenhouse gas. Increasing CO_2 concentration will lead to a rise in global temperatures and significant changes in the global climate. Potential solutions to avoid this are transitioning to renewable energy sources such as solar or wind energy, thereby reducing CO_2 emissions and recycling, capturing, and storing excess CO_2 from the atmosphere.

1.2 Carbon dioxide

Carbon dioxide is a colourless, odourless, tasteless gas heavier than air and a trace component of Earth's atmosphere. CO_2 is a linear, non-polar molecule featuring a central carbon atom covalently bonded to two oxygen atoms, and it is typically not toxic to humans at low concentrations. The molecular structure of CO_2 is quite stable due to strong double bonds between carbon and oxygen and the complete octet of electrons around the carbon atom. As a result, it has a high activation energy for decomposition and does not readily break down into its constituent elements.

Besides its natural occurrence, where its fundamental role in photosynthesis makes it essential for life, CO_2 can be synthesized by chemical processes for industrial purposes from the food and beverage industry to fire extinguishers, life jackets and many more. However, dealing with CO_2 is essential as a greenhouse gas because its geometry allows it to absorb energy radiated by Earth in wavelengths of the infrared range, causing it to vibrate and re-emit the infrared energy back towards Earth as heat. Therefore, CO_2's contribution to the greenhouse effect makes it very important to study various methods to remove it from our atmosphere.

1.3 CO_2 conversion methods

An excellent strategy to remove excess CO_2 from our atmosphere is to capture and store it or convert it into valuable chemicals. Many conversion methods can be employed to achieve this. In the following section, we will briefly discuss a few of the major processes here:

1. Direct air capture (DAC).
2. Bioenergy with carbon capture and storage. (BECCS)
3. Mineral carbonation.
4. Electrochemical CO_2 reduction. (ECR)
5. Thermochemical conversion.

1.3.1 Direct air capture (DAC)

DAC is a technology used to capture CO_2 from the air. This technology is regarded as an innovative solution to mitigate climate change as it can capture CO_2 from various sources, such as the atmosphere and diluted gases, irrespective of their origin and location.[5] The DAC process involves using engineered contactors filled with chemicals to repeatedly capture CO_2 from the air and release high-purity CO_2 that can be stored, used, or converted.[6]

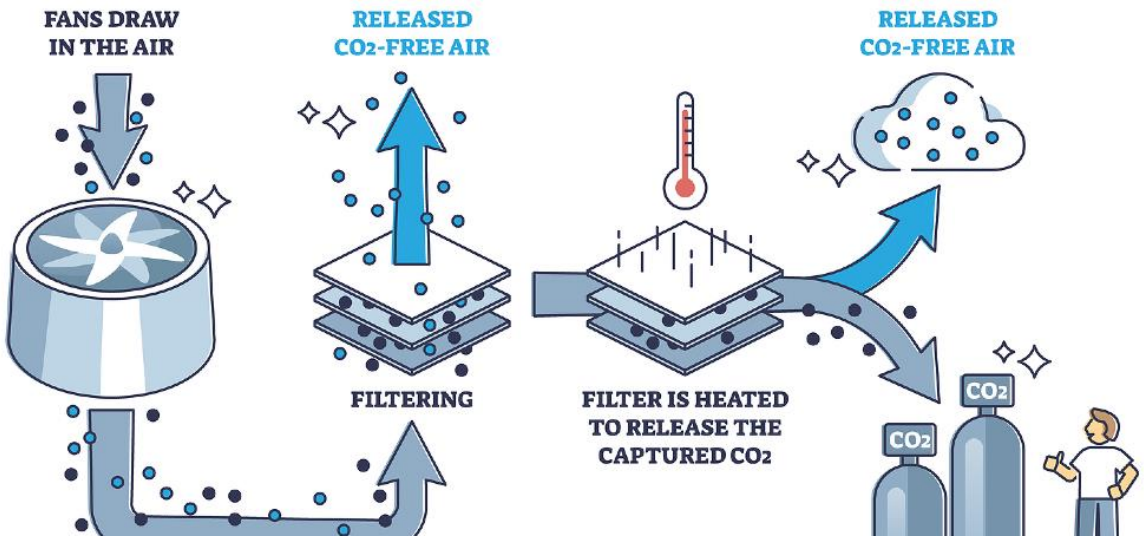

Figure 2 Schematic representation of DAC technology, where CO_2 from air is captured and stored to reduce its amount from the atmosphere or used for industrial purposes.[1]

Major commercial DAC processes are currently being developed, employing solid sorbents or liquid solvents for CO_2 capture, but many others are promising, albeit less developed, techniques. Solid sorbents involve the interaction of CO_2 molecules with porous materials; these materials can remove CO_2 from gas mixtures via physisorption or chemisorption.[1]

Various structures can be used as solid sorbents for DAC, including metal-organic frameworks (MOFs), zeolites, activated carbon, silica materials, carbon nanotubes, porous organic polymers, carbon molecular sieves and clathrates. On the other hand, liquid-based solvents, often amine-based, are often used for carbon capture.[7] In this process, CO_2 from the air is absorbed into a liquid solvent, creating a CO_2-depleted gaseous stream and a CO_2-rich liquid stream. This method requires a strong basic hydroxide solution to absorb CO_2 from the air.

DAC is a promising technology, but high initial costs and the need for specific site conditions limit current large-scale systems.[8] However, a recent approach to improving the performance of DAC is by m-DAC, which involves the use of thin-film composite membranes for separation and has several advantages over conventional DAC, including its energy efficiency, lack of need for special chemicals, scalability, and versatility in terms of installation locations if scaled rapidly DAC could be a viable option to meet climate goals.[9]

1.3.2 Bioenergy with carbon capture and storage (BECCS)

Bioenergy with Carbon Capture and Storage (BECCS) is a promising negative emissions technology that could help meet global warming targets. It is a technology that combines biomass use with carbon capture and storage.[10] BECCS works by first growing biomass, such as trees or crops, which absorb CO_2 from the atmosphere as they grow, leading to a net transfer of atmospheric CO_2 into the biomass. Next, this biomass is burned to generate electricity or heat, while CO_2 is emitted, which is then captured and stored, typically in geological formations, leading to the permanent removal of CO_2 from the atmosphere.

Most of the biomass used in heat and electricity generation derives from residual or waste products from forestry, agriculture, and municipal sources. There is further potential for growing energy crops such as Miscanthus, switchgrass, reed canary grass, rye, and giant reed grass[11]. Further, an increase in efficiency could be achieved by using high-performance solvents, heat recovery for energy regeneration, and greater recoverable heat from flue gas.

BECCS offers reliable, low-carbon electricity, making it a practical approach to decarbonizing the electricity sector and mitigating coal use. Nevertheless, BECCS faces challenges and controversies, including the need for extensive land for biomass cultivation, potential competition with food production and biodiversity conservation, and greenhouse gas emissions from biomass growth, harvesting, and transportation.[12]Ongoing studies aim to enhance BECCS performance by reducing pollutants, improving efficiency, and achieving CO_2 negativity. Despite technical feasibility, the primary obstacle to BECCS deployment lies in the lack of economic and political drivers.

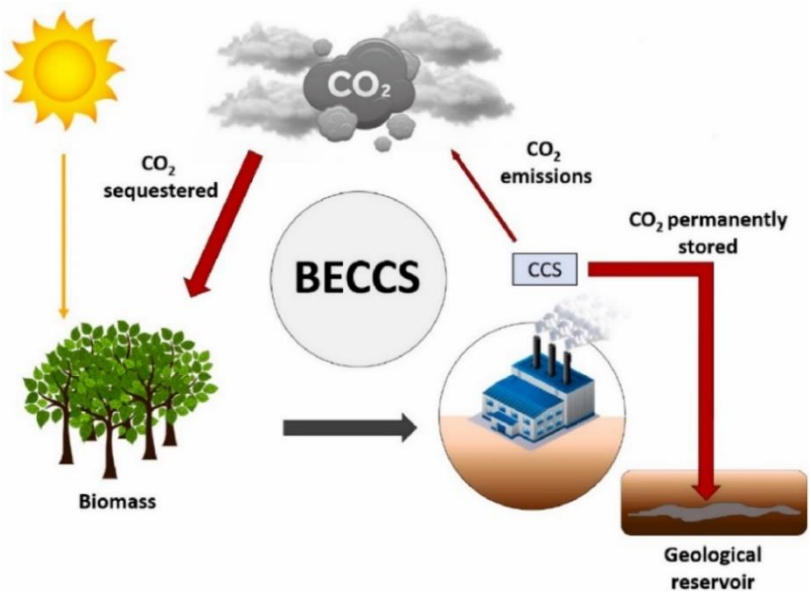

Figure 3 Illustration of carbon flow in BECCS technology where biomass is grown absorbing CO_2 and burnt for energy production, followed by storing the resulting CO_2 in geological formations.[13]

1.3.3 Mineral carbonation

Earth is the largest carbon reservoir, and the carbon cycle involves the movement of carbon between these terrestrial reservoirs, vegetation, atmosphere, and oceans in natural processes.[14] Soil and other terrestrial reservoirs are where carbon is held for the longest time; this could be replicated by Mineral carbonation, which involves CO_2 capture and sequestration in geological, oceanic, and mineral storage. This process involves injecting liquefied CO_2 into geological formations like storing fossil fuels in nature, causing a series of geochemical processes forming secondary minerals, making it a permanent solution for carbon storage.[15]

Mineral carbonation can be achieved by two main approaches: ex-situ and in-situ mineral carbonation. Ex situ mineral carbonation involves extracting rocks or minerals, after which CO_2 is introduced into these extracted minerals, usually in the form of a gas or dissolved in water, creating a reaction that converts the CO_2 into stable carbonate minerals[16]. On the other hand, in-situ, mineral carbonation involves pumping CO_2 directly into the subsurface, where carbonation occurs in the rocks or minerals. The injected CO_2 interacts with the rocks, forming carbonate minerals. Basaltic and ultramafic rocks are ideal for mineral carbonation.[17]

Both ex-situ and in-situ mineral carbonation have their advantages and challenges. Ex situ mineral carbonation allows for more control over the process conditions, resulting in potentially higher carbonation rates and greater carbon storage capacity. However, it requires significant energy for rock extraction, crushing, processing, and transporting materials to the

carbonation facility. On the other hand, in-situ mineral carbonation offers the advantage of utilizing the natural environment to reduce energy and transportation requirements. However, it may have limited access to suitable geological formations and the need to ensure effective CO_2 injection and distribution within the subsurface.[17, 18]

The current limitations of this technology are developing effective monitoring techniques to ensure that the injected CO_2 is securely fixed without any leakage. There is also a need to avoid the potential for acidification of underground water and marine sources, harming marine ecosystems. Care must also be taken to avoid the deformation of geological structures causing seismic activity due to the injection of CO_2.[19]

1.3.4 Electrochemical CO_2 reduction

Electrochemical CO_2 reduction (ECR) involves the transformation of CO_2 into value-added chemicals in an electrochemical cell. The ECR process involves three steps, all at the interface between the cathode and the electrolyte. First, CO_2 molecules adsorb on the electrocatalyst. Next, an electron/proton transfer occurs, breaking C-O bonds and forming an intermediate. Finally, these intermediates rearrange themselves into products and desorb from the catalyst's surface into the electrolyte. Harnessing renewable energy to power the electrochemical reaction is optimal for transforming CO_2 into value-added chemicals.[20]

Different products can be obtained through ECR, including carbon monoxide (CO), formic acid (HCOOH), methane (CH_4), methanol (CH_3OH), ethylene (C_2H_4), and other hydrocarbons and alcohols.[21] The selectivity of products obtained from the ECR largely depends on the catalyst used as an electrode and the reaction conditions. The first step of the ECR reaction is the activation of CO_2 to generate $CO_2^{\cdot-}$ and is the rate-limiting step, followed by further electron/proton transfer steps forming intermediates. Stabilizing the intermediates on the catalyst is crucial and determines the mechanisms and kinetics of the reactions.[22]

Metal electrodes are generally classified into four groups depending on the major product they form when CO_2 is reduced. Metals such as Pb, Hg, Tl, In, Sn, Cd, and Bi primarily produce formate; Au, Ag, Zn, Pd, and Ga produce CO; Ni, Fe, Pt, and Ti exclusively reduce water to H_2. Copper is the only metal electrode that stands out in ECR, producing hydrocarbons, aldehydes, and alcohols with substantial Faradaic efficiencies[22]. ECR is a balancing act between finding an electrode material that reduces CO_2 with high activity and selectivity while being inactive for competing reactions such as HER. The pH of the solution is also an important factor because the pH directly impacts the HER and the solubility of CO_2.[23]

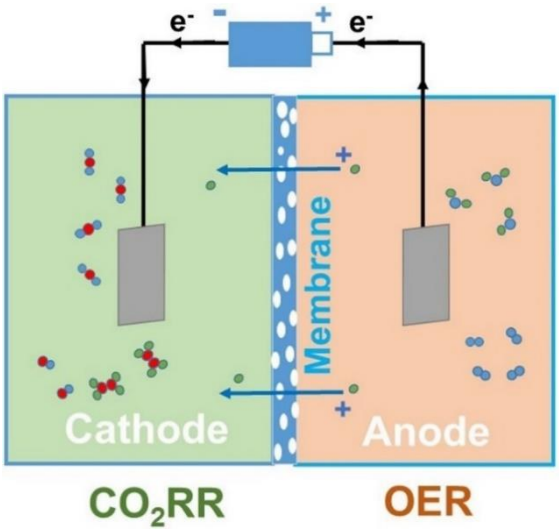

Figure 4 Schematic illustration of electrochemical reduction of CO_2 in an aqueous system.[21]

Current research efforts are focused on investigating new types of catalytic active sites to increase the efficiency of the ECR process. Many studies have shown that the geometry, morphology, roughness, and size of catalyst particles greatly impact activity and selectivity. Many new catalysts are under study where the properties mentioned above could be tailored; these new catalysts include nanomaterials such as nanoparticles, nanotubes, nanowires and nanofilms, hybrid metals, oxide-derived metals, metal porphyrins, heteroatomic carbon-based films, core/shell structures, and metal clusters.[24]

The electrochemical CO_2 reduction process offers several advantages. It can operate at ambient temperature and pressure, making it energetically favourable compared to traditional chemical processes. However, several challenges and limitations are regarded to electrochemical CO_2 reduction. For instance, the low reactivity and stability of CO_2 molecules make their electrochemical reduction kinetically challenging, requiring the development of efficient catalysts and reaction conditions. Catalyst design and optimization play a crucial role in enhancing selectivity and efficiency.[25] While there are still challenges in cathode development for CO_2 reduction, the anode also requires attention because a large portion of the voltage drop in a CO_2 electrolyzer occurs due to the oxygen evolution reaction.

Another limitation of ECR is the scalability and cost-effectiveness of the process. Electrochemical CO_2 reduction is currently conducted in laboratory-scale setups, and scaling it up for industrial applications poses technical and economic challenges.[26] Developing cost-effective catalyst materials and reactor designs is essential for commercial viability.

1.3.5 Thermochemical CO_2 reduction.

The catalytic conversion of CO_2 to fuels or chemicals holds great significance for sustainable energy and the environment, although it is challenging due to the high stability of CO_2.

Thermochemical CO_2 reduction offers a promising approach to removing excess CO_2 from the atmosphere and converting it into valuable chemicals and fuels. This process initiates with CO_2 reduction to CO by the reverse water gas shift reaction,[27] which produces syn gas. This syn gas can be used as a feedstock to long-chain hydrocarbons or small molecules such as methane (CH_4) and methanol (CH_3OH) or yield long-chain hydrocarbons like in the Fischer-Tropsch reaction.[28]

Under high-pressure conditions, different catalysts can generate various alcohols and hydrocarbons, such as ethanol and gasoline-range hydrocarbons. Active catalysts for producing CO and CH_4 have included different precious and nonprecious transition metals supported on oxides. Selectivity to desired products has been improved by catalyst modification strategies such as tuning the particle size of metal, changing the oxide support, or using bimetallic catalysts.[29, 30] However, there are challenges with the thermochemical CO_2 reduction process. A significant issue is the source of hydrogen. The current market derives 99% of hydrogen from fossil fuels, primarily through methane reforming, and new HER catalysts need to be developed for the commercial production of hydrogen through electrolysis. Another significant issue is the high energy requirement to drive the reaction, which can make the process cost-ineffective. The stability and efficiency of catalysts at high temperatures pose additional variables.[29]

The selectivity of the reaction, or the ability to control the output to get the desired product, is another problem since CO_2 can be reduced to a variety of substances, including carbon monoxide (CO), methane (CH_4), and a variety of other hydrocarbons and alcohols. To improve the activity, selectivity, and stability of the catalyst for the thermochemical conversion of CO_2, identification of the active site and the corresponding reaction pathway is necessary, which requires various characterization techniques.[31] One promising strategy is using nanostructured catalysts, which can enhance reaction rates and selectivity due to their high surface area and unique properties at the nanoscale. Ongoing research is focused on overcoming these challenges by developing advanced materials for catalysis, new reactor designs, and integrated systems that can harness renewable energy more efficiently. Combining thermochemical CO_2 reduction with carbon capture and storage (CCS) technologies could further enhance the overall CO_2 mitigation impact. Nevertheless, substantial research and development are needed to address the current challenges and advance towards efficient, large-scale applications of this promising technology.[32]

2 Metal-Organic Frameworks for catalysis

2.1 Metal-Organic Frameworks

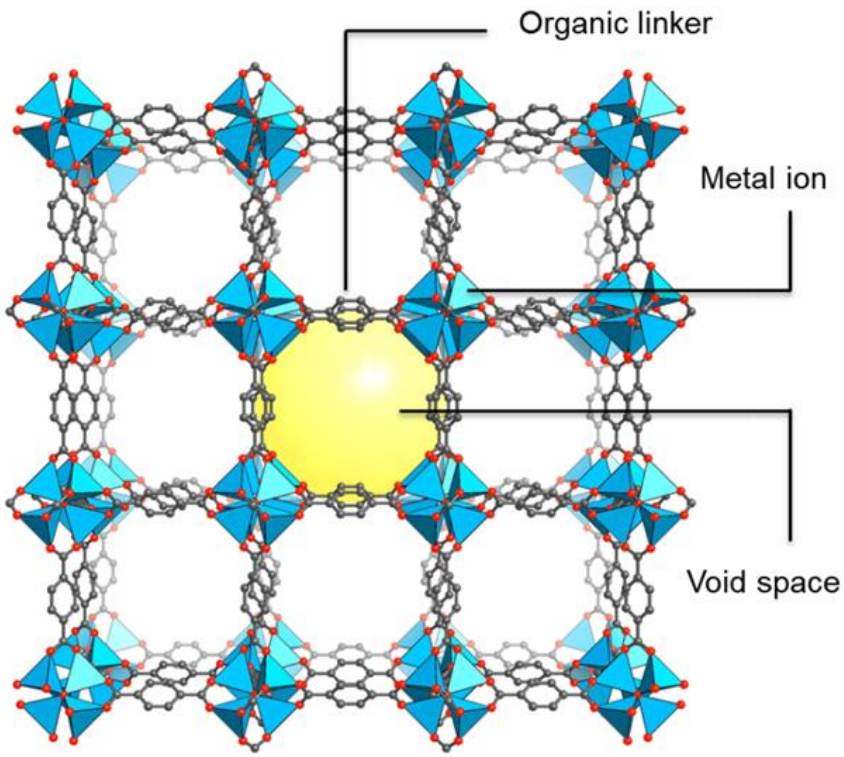

Figure 5 Example of MOF structure, showing its porous nature and secondary building units: Organic linkers and Metal clusters.

MOFs are inorganic-organic hybrid materials constructed by combining metal-oxide nodes (clusters) with carboxylate-type organic linkers. These structures form highly crystalline and

ordered materials with pores.[33] MOFs have attracted research interest due to their unique properties and diverse applications in gas storage, separation technologies, catalysis, biomedicine, and molecular sensing.[34] The design of MOFs involves combining metal nodes with various linkers, offering a wide range of materials with modular properties. Different combinations of metal nodes (such as Cu, Zn, or Zr) and linkers with varying connectivity, length, and functional groups result in various pore shapes and sizes, influencing chemical and thermal stability and adsorption.[35]

MOFs can incorporate metal species coordinated to the functional groups of the linkers, forming well-defined metal moieties. These moieties can aggregate and form nanoparticles within the porous MOF structure through reductive treatment. Alternatively, existing nanoparticles can be encapsulated within MOFs. This flexibility allows for creating of numerous MOF structures with tailored properties for specific applications. The synthesis of MOFs often involves solvothermal methods, where the metal precursor, linker, and suitable solvent are mixed under specific conditions. The resulting MOFs initially contain solvent molecules in their pores, which can be removed to create permanent porosity. MOFs can be viewed as an ordered array of molecules, but the assembly and composition of MOFs can significantly affect the electronic properties of the constituents. The interplay between linkers and metal ions/clusters results in materials with unique properties relevant to optics, photocatalysis, and other applications where the MOF structure and composition influence localized states.[36]

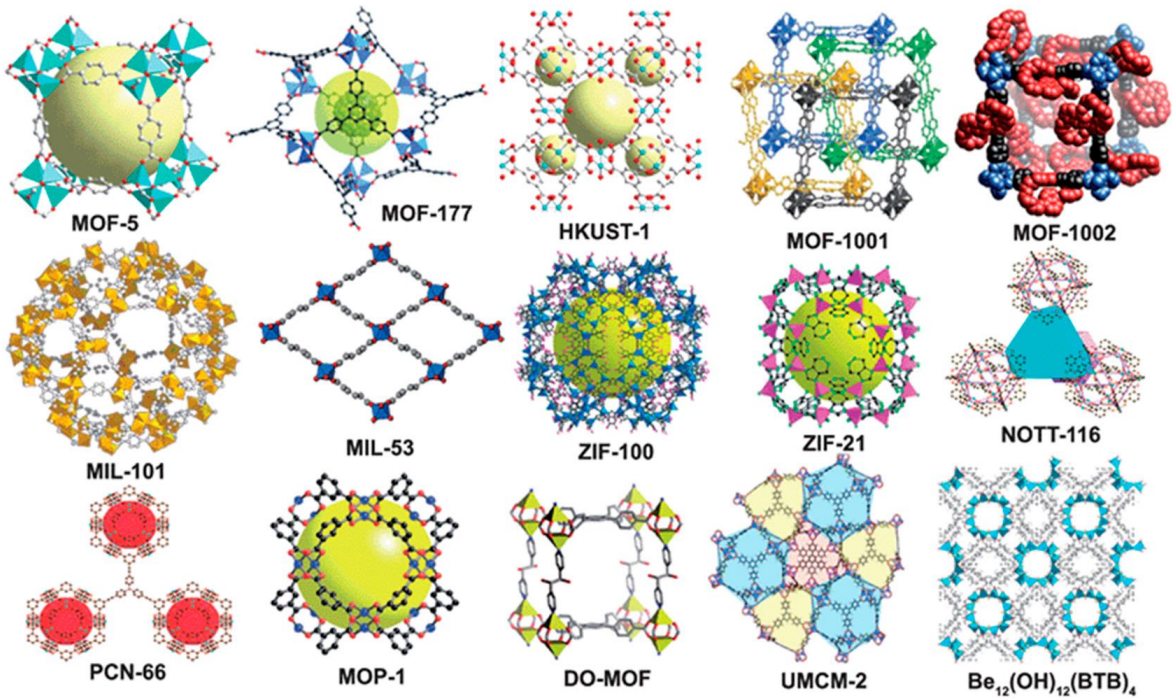

Figure 6 Examples of Metal-organic framework structures.[37]

While computational methods are suitable for predicting and exploring MOF properties, more synthetic approaches are available to modify and create novel organic linkers than inorganic clusters. Modifying organic linkers enables fine-tuning of the bulk material's properties. However, the electronic structure of most MOFs does not significantly impact the local electronic structure of catalytically active sites. Considering the vast chemical space and diverse applications of MOFs, theoretical approaches like density functional theory (DFT) play a crucial role in guiding synthetic efforts and understanding the chemical origins of observable MOF behaviours.

Furthermore, collaborations between theory and experiment accelerate the discovery and development of functional materials for various technologies, including renewable energy, catalysis, and low-energy chemical separations.[38]

2.2 Application of MOFs

In recent years, functional metal-organic framework materials have increased relevance. With their self-assembling ability and versatility, MOFs can incorporate an array of metal ions/clusters and organic linkers that are chemically, optically, magnetically, electrochemically, biologically, and catalytically active. Furthermore, the porosity of these

MOFs provides an ability to encapsulate various guest substrates, ranging from gases, ions, and nanoparticles to biological chemicals and dyes. This unique combination of properties makes MOFs an extremely versatile inorganic-organic hybrid material. As a result, MOFs have found applications across many fields, such as gas storage, separation processes, Sensing applications, catalysis, and medical fields. In the following subsections, we will discuss a few of these applications.

2.2.1 MOFs for gas storage and separation

The search for sustainable and efficient energy solutions has led to exploring innovative materials, particularly for gas storage and separation.[39] MOFs have emerged as crucial materials for these applications due to their ultra-high porosity, tunable pore size, and surface functionalization. These characteristics allow their structures and properties to be designed and optimized to store and separate gases effectively. Gas fuels like H_2 and CH_4 present significant transportation, storage, and conversion challenges, requiring energy-intensive conditions. Similarly, olefins and aromatic hydrocarbons, which serve as significant feedstocks in the chemical industry, necessitate energy-intensive processes for their production and purification.[40] MOFs offer an alternative solution to these issues by enabling inexpensive, safe, and portable storage and transportation under moderate conditions, significantly reducing energy consumption and contributing to environmental sustainability.

Compared to traditional porous adsorbents like zeolites and activated carbons, MOFs have shown record uptake capacities for gases like H_2, CH_4, and C_2H_2. This is largely due to the ability to tune MOFs' structures, create optimal framework structures and porosities, and immobilize functional groups. Many MOFs have demonstrated high gravimetric storage capacities due to their large surface areas, some surpassing 6000 m^2/g. A MOF's maximum theoretical surface area can be as much as 14600 m^2/g, leading to future expectations of greater gravimetric gas storage capacities.[41] However, in practical applications such as vehicle fueling, a high volumetric gas storage capacity is more critical than a gravimetric capacity. Consequently, rather than just pursuing ultra-high porosity, optimizing framework structures and pore/cage sizes to target high volumetric gas uptake capacity must be focused on.

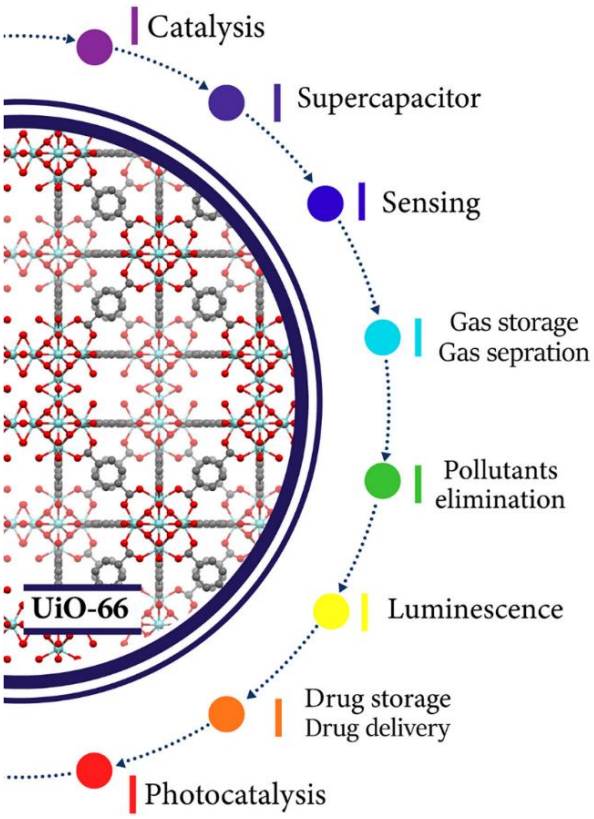

Figure 7 Various applications of UiO-66 MOF.[42]

Fine-tuning MOFs' pore sizes has also allowed for greater exploration of MOFs for gas separation and purification. MOFs' Functional groups can act as binding sites for gas molecules, enhancing their gas storage and separation capacities. Open metal sites within porous MOFs can also play crucial roles in gas storage under low pressure.[43] Nonetheless, MOFs with high densities of open metal sites might not always be advantageous due to the impracticality of releasing all the gas molecules under a vacuum and the need to maintain specific pressures within MOF-filled tanks.[44]

For hydrogen storage, MOF-filled cryo-temperature H_2 storage tanks have demonstrated higher H_2 capacities and working temperatures than traditional cryogenic liquid H_2 tanks. However, room-temperature H_2 storage with MOFs remains a significant challenge due to weak interactions like van der Waals forces. In contrast, room-temperature methane storage with MOFs is more feasible, although there are still practical issues to be addressed.[45]

Regarding gas separation, MOFs have revolutionized gas separation due to their unique pore features. Technological advances have rapidly progressed in this field, particularly in the last three years. For instance, MOFs are used as adsorbents or membrane materials for CO_2 separation, with efforts concentrated on enhancing MOFs' affinity for CO_2 or O_2.[46] This

results in enhanced selectivities in post-combustion capture, direct capture from the air, and oxyfuel combustion. Some CO_2-selective MOFs modified by alkylamines exhibit exceptionally high CO_2 working capacities with good recyclability at the required capture conditions.[47] Furthermore, the performance of these materials remains unaffected by moisture, which strongly implies their potential for application in real industrial cases. If improvements can be made on their long-term stability and resistance to minor components like SO_x and NO_x in flue gas, and reductions can be achieved in their regeneration energies and synthesis costs, these MOF adsorbents are likely to play a crucial role in CO_2 capture.[48]

Metal-Organic Frameworks' tunable pore size and shape, combined with a high surface area and adjustable porosity, ability to adsorb gases at low pressures/concentrations makes them ideal for direct and selective detection of organic and inorganic compounds, trace materials such as explosives, chemical weapons, and volatile organic compounds[49]. Typically, MOF-based chemical sensors require a physical interface between the MOF and a device so they are layered on surfaces for diverse applications. These sensors' effectiveness depends on the MOF films' characteristics, such as their crystal size and thickness, as these elements influence the electron-transfer dynamics and adsorption capacity.[50] Various types of MOF-based sensors have been developed and tested.

Some examples of using MOFs as chemical sensors are: quartz microbalance was coated with a MOF to monitor the uptake of different hydrocarbons, a microcantilever coated with HKUST-1 allowed for the detection of substances such as water vapour, alcohols, and CO_2.[51] Luminescent MOFs have been deployed in sensing applications to identify explosives and other hazardous molecules, such as organic phosphonates—known surrogates for nerve agents—by using IRMOF-1,[52, 53] which can trap and concentrate them. Another is a glucose sensor developed with a ZIF-8 EBFC sensor showed a consistent response to glucose concentrations ranging from 1 to 10 mM, facilitating continuous glucose monitoring for up to 15 hours.[54]

Coupled with these results, the variety of MOF structures suggests significant potential to enhance both the uptake and selectivity for specific analytes. Nonetheless, several challenges need to be addressed, such as the need for water-stable MOFs in aqueous environments, improvement of electronic conduction in MOFs, a requirement for larger surface areas and electronic conductivity for electronic-based sensing applications, and the issue of differentiating between molecular species of the same molecular mass. Despite challenges to overcome, the unique properties of MOFs present exciting opportunities for their application in various fields, including healthcare and environmental monitoring. Besides chemical sensing, MOFs are also used in various sensor technologies, from electrochemical to optical and electromechanical. [5, 55]

2.2.2 MOFs for water purification

The increasing global population, rapid industrialization, and climate change impact stress the importance of efficient water purification methods. However, water security and

providing clean water is still a challenge to our society, which is made more difficult due to the introduction of various pollutants into our water sources.[56] These pollutants range from heavy metal ions to pharmaceuticals, personal care products[57], fluoride, pesticides, and herbicides, many of which are toxic or carcinogenic. The presence and consumption of this polluted water pose significant risks to the environment, ecosystem, and human health.

Techniques for treating wastewater containing these pollutants have traditionally relied on a range of physical, chemical and biological processes, such as chemical precipitation, biological degradation, adsorption, catalytic/photocatalytic degradation, flocculation, flotation, coagulation, ion exchange, membrane filtration, and electrochemical treatment[58]. However, these methods often require expensive chemicals, harsh operating conditions, multiple steps, and high energy needs. Nanoporous materials, such as metal-organic frameworks, with their unique structural and performance attributes, are promising tools to address this environmental crisis. Their high crystallinity, high porosity and large specific surface area make them highly suitable for water treatment applications, outperforming many other nanoporous materials.

Water molecules can attack the metal-organic coordination bonds, break the ligand-metal bonds, change the crystal phases, and ultimately cause the MOFs' structure to collapse.[59] This underlines the importance of water stability for their potential application in water purification and depends on factors such as the bond strength of the metal linker. Many MOFs degrade in aqueous environments, while some maintain their structural integrity, and others have not been completely investigated yet. To evaluate the stability of MOFs in an aqueous solution, compare certain properties before and after interacting with water. Typical tests include analyzing the crystal structure, porosity, and surface area.[60] The pH level of the solution also plays a significant role in the stability of MOFs. In recent years, the creation and development of water-stable MOFs have been a focal point in research, leading to numerous MOFs exhibiting enhanced structural stability against water, organic solvents, high-temperature steam, and extreme pH conditions.[61]

MOFs can be used in water purification processes in three different technologies, such as (1) adsorption due to porosity, (2) As catalysts in oxidation processes, and (3) As membranes for separation.

Adsorption: MOFs are excellent adsorbents and can remove hazardous compounds from water due to their high surface area, tunable porosity, and various functional groups. The design of the MOFs can be tailored to optimize adsorption performance for different types of water pollutants, such as the target pollutant's size, shape, and chemical properties.[62] The adsorption capability of MOFs can be because of various types of interactions, such as π-complexation, hydrogen bonding, acid-base interaction, and π-π interaction.[42] Most importantly, the adsorption capacity of MOFs can be regenerated by washing or heat treatment, allowing for reuse and improving the sustainability of the water purification process.

Catalysts in oxidation processes: Another promising application of MOFs in water treatment is as catalysts, including Fenton reactions, photocatalysis, and photo-assisted applications. These MOFs, employed in advanced oxidation processes, usually have redox-active metal centres or can house other catalytic species that generate reactive oxygen species, effectively oxidizing a wide range of organic contaminants. Additionally, MOFs that respond to light can be used in photo-Fenton or photocatalytic reactions, using light energy to degrade pollutants.[56]

Fenton Process: The Fenton method uses Fe(II) to trigger H_2O_2 and produce highly reactive hydroxyl radicals that can oxidize many organic pollutants; these Fe-MOFs have demonstrated that an efficient FeII/FeIII redox pair is necessary for Fenton reactions. Several other Fe-MOFs have also shown potential in Fenton reactions.[63] They have performed well in degrading pollutants like methylene blue and have shown stability over multiple reaction cycles. However, despite efforts to enhance its stability and performance, this method has limitations, such as requiring low pH, high usage of H_2O_2 and iron catalyst and suffering from iron leaching.[64]

Photocatalysis: This process uses light to initiate chemical reactions and degrade hazardous compounds and is suitable for MOFs as they can function as semiconductors. They can be excited to generate electron-hole pairs to facilitate redox reactions.[65] A key challenge in this area is the rapid recombination of photogenerated electron-hole pairs, limiting efficiency. Strategies such as combining MOFs with noble metals or forming heterojunctions with other semiconductors have been explored to overcome this limitation.[66]

Membranes for separation: MOFs have also found applications and demonstrated excellent performance in removing various pollutants, including heavy metals, dyes, salts, and microorganisms.[67] Due to their tunable porosity and high permeability, MOFs can be integrated into membranes to separate toxic substances from water streams. MOF membrane can be synthesized in Two primary methods: continuous growth and composite systems.

Continuous growth includes solvothermal and layer-by-layer growth, resulting in pure MOF membranes. However, the solvothermal synthesis method can lead to the formation of defects due to the imperfect intergrowth of different MOF crystals. On the other hand, layer-by-layer synthesis allows for more uniform growth of MOF layers.[68] Composite systems MOFs are synthesized in powdered form and combined with polymeric binders to form mixed-matrix membranes. Although these membranes have a wide range of MOF loadings, at lower MOF loadings, the membrane properties closely resemble the properties of the polymer, and at higher MOF loadings, the membrane properties reflect those of the MOFs.

In addition to these primary applications, ongoing research explores the potential of MOFs for other water treatment technologies. For example, MOFs could be used in capacitive deionization, a technique that uses electric fields to remove salts from brackish water or seawater, or in removing radionuclides from nuclear wastewater.[69] Overall, the versatility and tunability of MOFs make them a promising class of materials for addressing the global challenge of water purification.

2.2.3 MOFs for carbon capture

Metal-organic frameworks have emerged as promising carbon dioxide capture materials due to their unique advantages over traditional materials such as ionic liquids, zeolites, porous carbons, porous organic polymers, and covalent organic frameworks. The current industry standard for CO_2 capture, amine scrubbing,[70] is plagued by issues such as the corrosive nature and volatility of amines, their tendency to decompose, and the high energy cost of regeneration.[71] MOFs present a more efficient and cost-effective alternative with their tailorable and functional structures, high chemical tunability, and compatibility with other materials.

The effectiveness of MOFs in CO_2 capture is attributed mainly to their unique structural and chemical properties. The interaction between the MOF framework and CO_2 molecules plays a crucial role in CO_2 capture, with stronger interactions resulting in higher CO_2 uptake capacities, particularly at low loading pressures. Selective adsorption, an essential requirement in CO_2 capture applications,[43] can be achieved through kinetic or thermodynamic separation. Kinetic separation relies on size/shape exclusion, as demonstrated by MOFs like MIL-96 and $Zn_2(cnc)_2(dpt)$, where the size of the pores in the framework allows molecular diffusion and the free OH groups inside the pores attract CO_2. However, the small pore size stops CH_4 adsorption.[72, 73] However, thermal separation depends on physical properties such as polarizability and quadrupole moment, as in the case of Mg-MOF-74, which achieves CO_2 separation over CH_4 due to exposed metal cation sites that improve selectivity toward CO_2.[74]

MOFs can be tailor-made for CO_2 capture through the functionalization of ligands.[75] The most effective MOFs employ alkyl amine-functionalized pores that selectively react with CO_2, forming covalent C−N bonds.[76] This can be achieved either through post-synthetic functionalization of MOFs by introducing an NH_2 group or direct synthesis of MOFs containing NH_2-based linkers. Introducing amide groups into MOF can improve CO_2 uptake because CONH groups can form hydrogen bonds with CO_2. This is evident in the pores of a Cu-based MOF, which shows higher CO_2 uptake, enhances adsorption heat, and increases selectivity compared to similar MOFs that contain alkyne groups instead.[77]

Despite their promise, MOFs face several challenges in CO_2 capture applications. These include the need for high CO_2 selectivity in the presence of moisture, water, and acidic gases and improved stability.[78, 79] When considering large stationary sources like power plant flue gas for CO_2 capture, addressing the preferential adsorption of more polar or higher binding energy gases like water or acidic gases over CO_2 on the open metal sites of MOFs is essential.[80, 81] Strategies have been developed to improve MOFs' water and acid stability, but unexplored MOFs may be better suited for this application.

Balancing functionalization while maintaining crystallinity and desired porosity is challenging, as some strategies may lead to reduced surface areas or pore volumes.[75] Additionally, capturing CO_2 at low partial pressures remains a challenge due to weak CO_2-

framework interactions. Combining multiple strategies, such as creating open metal sites, controlling pore size, and amine-functionalization, can help MOFs achieve the desired CO_2 capture ability. Although extremely high surface area and pore volume are not mandatory for CO_2 capture at low pressures, sufficient binding sites, usually determined by the surface area and pore volume, are still necessary.[82, 83] In addition to the adsorption performance, the regeneration cost and the influence of water and other impurities should be carefully considered for practical use.

2.2.4 MOFs for catalysis

Metal-organic frameworks have attracted considerable interest and achieved impressive advancements in catalysis. These advancements can be attributed to their highly porous structure and large surface area, which allow for spatial separation of catalytic sites and efficient molecule transportation.[84] These materials present unique characteristics not commonly found in conventional inorganic or organic materials; as a result, MOF-based catalysts have been extensively studied across various applications, including thermo-catalysis, photocatalysis, and electrocatalysis. With their intrinsic catalytic activity, MOFs offer opportunities for the rational design of new catalytic solids and have three different sites that provide intrinsic catalytic activity, as shown in Figure 8: 1. open metal sites 2. Functionalization of linkers. 3. Guest materials.[85]

Open metal sites (OMS): OMS are a feature of MOFs, typically referred to as metallic nodes and serve as the core structure of the MOF. They result from unsaturated metal ions only partly coordinated by the organic ligands in the MOF structure.[86] OMSs are highly reactive due to their unsaturated coordination environment, allowing them to interact with various substrates and often act as active sites for catalytic reactions; they are similar to the metal centres in traditional catalysts.

Because of the MOF structure, these nodes are well dispersed and accessible, and their catalytic activity can be adjusted by varying the metal ions used in the MOF. The interaction between these metallic nodes and guest species can influence the activity and selectivity of the MOF catalyst, contributing to its overall performance. They are beneficial in catalysis, gas storage, and separation applications. In heterogeneous catalysis, OMSs can act as active sites for various reactions, including oxidation, reduction, and coupling reactions.[86]

Mainly, this interaction takes the form of electronic metal-support interactions. A common approach in MOF catalysis involves leveraging unsaturated metal oxide nodes, also known as open metal sites. These sites are created when the metal ion has a lower coordination number than theoretically possible, usually due to the removal of solvent molecules coordinated during synthesis. For instance, in an ideal UiO MOF, Zr-oxide nodes are fully connected by 12 linkers, suggesting that the open metal sites, potential Lewis acid centres, are theoretically entirely occupied by the linkers. However, UiO MOFs often contain coordination defects due to the use of modulators during synthesis. The type and concentration of these modulators

can significantly influence the number of these defects and, therefore, the formation of open metal sites. This results in enhanced Lewis acid catalytic activity of the MOF.[87-89]

Moreover, the metal nodes' hydroxyl (-OH) groups provide anchoring sites for additional metal ions. Metalation of these –OH groups, as in the case of UiO MOFs, is a practical approach to incorporating various active metals into the MOF structures.[90] This method expands their application potential, making them suitable for various high-temperature gas-phase reactions. Therefore, the metallic nodes in MOFs play a pivotal role in their catalytic activity, making them a versatile tool in catalysis, with their function and efficiency adjustable through various modification techniques.

Functionalized linkers: linkers inside Metal-Organic Frameworks significantly impact their catalytic properties and functionality. Linkers can be functionalized in ways: pre-synthesis functionalization and post-synthetic modification.

1. ***Pre-Synthesis Functionalization:*** This process involves adding functional groups to the linkers before the MOF synthesis. This strategy allows for the attachment of many functional groups depending on the MOF's role. However, this approach has many challenges. The functional group could coordinate with the metal ion or reacts with synthesis reagents, inhibiting the desired framework formation or changing the linker's solubility and thermal stability.[91, 92]

2. ***Post-Synthetic Modification:*** Post-synthetic modification is a strategy for functionalizing MOFs after synthesis. This approach adds functional groups to the linkers after the MOF has been synthesized, avoiding the limitations of pre-synthesis functionalization.[93] This modification can be achieved in many ways like, modifying the organic linkers or metal ions or indirectly by encapsulating or grafting functional species onto the MOF structure, Post-Synthetic Deprotections, Solvent-Assisted Linker Exchange, Post-Synthetic Exchange (PSE), where the existing linker in the MOF is replaced with a new one while maintaining the MOF topology.

The functionalization of linkers in MOFs plays a crucial role in their catalytic activity. Both pre-synthesis and post-synthetic functionalization provide advantages and challenges for MOF synthesis, contributing to developing MOFs with varying functionalities suitable for various applications, including catalysis.

Encapsulation of guest materials: Many relevant industrial processes rely on the use of metal nanoparticles (MNP), and their catalytic performance in selectivity is highly related to the size of the metal nanoparticle employed.[94] Achieving a particle size distribution close to the optimal particle size for the reaction so that both activity and selectivity are maximized is very important. Metal nanoparticles encapsulated within MOFs provide a great opportunity to enhance their catalytic properties and use MOFs as hosts for metal nanoparticles. MOFs can incorporate various active species within their pores to catalyze a wide range of reactions efficiently and selectively.[95]

MOFs play different roles in these composites, such as (i) stabilizing MNPs within pores and controlling the particle size and distribution; (ii) assisting in the selectivity of the reaction by acting as a molecular sieve; (iii) altering the electronic properties of MNPs by controlling their electronic density and the electron charge transfer between the MOF and an MNP; (iv) catalyzing one-pot tandem reactions in which both the MOF and MNPs act as separate active sites in their respective reactions.[84]

These guest materials can be encapsulated through synthetic or impregnation strategies, each offering unique advantages and restrictions. This method encapsulates catalysts within the MOF, allowing for their active participation in catalytic reactions. The impregnation method is used when the catalyst is unstable under MOF synthesis conditions. This method dissolves the catalyst in a stable solvent, which is then allowed to diffuse through the MOF pores. However, the impregnation method has drawbacks, such as limited catalyst loading, potential leaching, and lower homogeneity than synthetic encapsulation.

Additionally, the porous nature of MOFs can be leveraged to encapsulate larger molecular guests than typically allowed by the MOFs' pore size. Furthermore, further understanding is necessary to exploit MOFs' full catalytic potential despite these advancements. This includes developing methods to prevent leaching in composites synthesized by impregnation and a deeper exploration of the role of guest materials in catalysis.

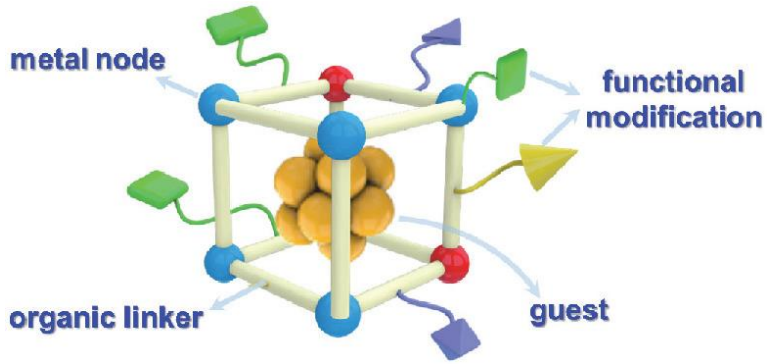

Figure 8: Active sites in a functionalized MOF[96].

In addition to the three intrinsic catalytic sites in a MOF, defect sites also play an important role. They refer to missing or irregular components in the ideal MOF structure. These defects can be missing linker units, metal ions, or vacancies in the organic or inorganic components of the MOF. Defect sites can significantly influence the properties of MOFs, including their stability, porosity, and catalytic activity. Defects can create additional active sites for catalysis, enhance the accessibility of the MOF interior, and modify the electronic structure of the MOF. Defect engineering in MOFs is a powerful strategy for tuning their properties for specific applications.

The use of MOFs as precursors for synthesising advanced catalytic materials is a clear response to the issues highlighted above and, so far, has been very successful. The unique structures obtained from the transformation of MOFs via thermal decomposition have opened a new field for synthesising highly advanced heterogeneous catalysts. Tunable porosity, unprecedented dispersion, and high metal loading with exceptional particle size control can be easily achieved. In conclusion, MOFs offer great opportunities for rationalising new catalytic solids, as highlighted by the unprecedented number of publications over the past decade. However, challenges remain in the practical application of MOF catalysis. Catalyst deactivation, thermal stability, leaching of components, and understanding the catalytic activity, selectivity, and stability of MOFs under reaction conditions require further investigation.[97-100]

2.3 UiO family of MOFs

The potential application of Metal-Organic Frameworks as catalysts or supports needs high thermal and chemical stability and mechanical robustness as a prerequisite. However, many initially developed MOFs' have relatively weak metal-ligand coordination that reduced their stability, temperature and solvent resistance compared to other porous materials like zeolites. As a result, even though tens of thousands of MOFs are reported, only a handful are helpful for practical catalysis applications. Tetravalent metals (Ti^{4+}, Zr^{4+}, Hf^{4+}, or Ce^{4+}) and carboxylate linkers have drawn particular attention due to their high stability.[101-103] There are two main reasons for the excellent chemical stability of M^{4+}-based MOFs. Firstly, the strong M^{4+}–carboxylate interaction contributes to the chemical stability of the MOF. Second, more ligands are needed to balance the charge on the tetravalent metals, leading to a high connection number with improved stability, high crystallinity, and diverse topologies. Zirconium-based MOFs are widely used for this reason and because of the ease of defect creation facilitated by the high degree of connectivity between the metal and organic linkers. Some of well know Zr-based MOFS are UiO-66, UiO-67, MOF-808 and NU-1000.

The UiO-67 MOF, where UiO stands for Universitetet i Oslo, was employed in this study to investigate the CO_2 hydrogenation reaction. The UiO-67 MOF is derived from UiO-66, a Zi-based MOF and is regarded as one of the most reported thermally and chemically stable MOFs. This MOF comprises $Zr_6O_4(OH)_4$ clusters as secondary building units and terephthalate (1,4-benzene dicarboxylic acid (BDC)) ligands, with each cluster connected to 12 neighbouring clusters via BDC linkers and has two types of micropores within, namely tetrahedral and octahedral.[104-106] Due to the strong acid and base properties of Zr^{4+} ions in the clusters and carboxylate ligands, the resultant coordination bonds make UiO MOFs chemically and thermally stable in organic solvents and water.

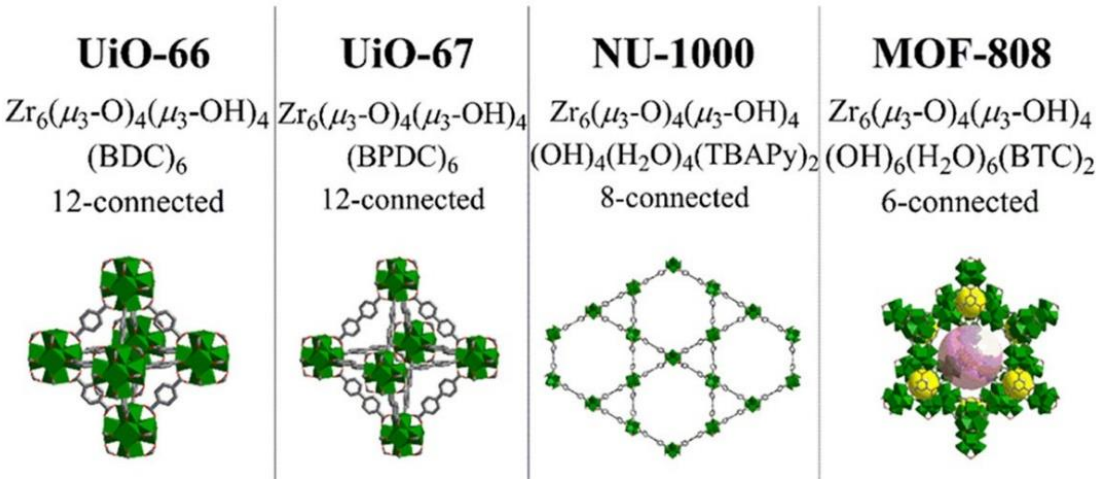

Figure 9 Zr-based MOFs with denotations, formulas and their structures [107]

When the length of the linkers is increased, the pore size and surface area of MOFs are also increased, giving us new MOF structures. In the case of UiO-66, replacing the BDC linkers with 4,4'-biphenyl dicarboxylate (BPDC) or terphenyl-4,4'-dicarboxylate (TPDC) linkers gives us two new MOFs, UiO-67 and UiO-68 respectively. The Brunauer-Emmett-Teller surface area and pore volume of these two MOFs were significantly higher when compared to the original UiO-66 MOF. Both UiO-66 and 67 MOFs are stable when synthesized even with missing liker defects due to the high connectivity of the framework that can maintain the crystallinity even with the loss of few linkers. They can be dehydrated upon activation at high temperatures (~250°C) and rehydrated when water vapour is introduced. The missing linker sites can also adsorb water on the zirconium defect sites as hydroxyl (OH-) and water (H_2O).[108-110]

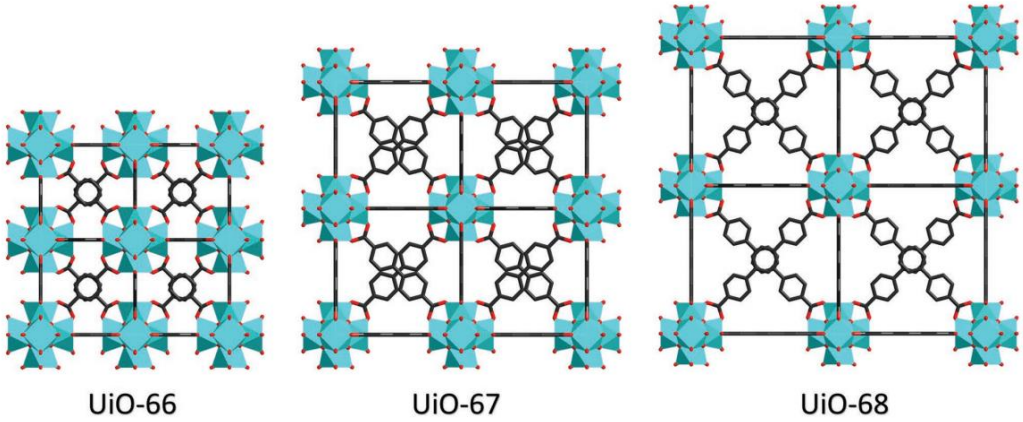

Figure 10 Structures of UiO-66, 67, and 68 MOFs illustrating the increased size due to different linker lengths.[111]

2.4 State of CO_2RR and the Role of Computational Analysis in CO_2RR

This dissertation elucidates the critical role of computational analysis in understanding and optimizing reaction mechanisms, particularly considering the current challenges in catalysis. It has been demonstrated throughout this research that a combined approach, which includes density functional theory calculations in concert with experiments, considerably improves our understanding of the catalytic processes. This synergistic method proves especially valuable when studying chemical reactions in complex structures such as MOFs, where traditional experimental techniques alone may struggle to render precise mechanistic insights. The present study illustrates this as we take advantage of the combined approach to scrutinize the dynamic role of the Pt-UiO-67 on the CO_2 hydrogenation reaction, emphasizing the necessity for comprehensive computational modelling tools.

Previous research on designing catalysts for CO_2 hydrogenation has shown that on Cu-based catalysts, the presence of ZrO_2 or isolated Zr moieties close to Cu facilitates methanol formation by forming low-coordinated Lewis acidic Zr-sites[112-114]. Formate and methoxy groups are also observed at sites at the interface of Cu/Al_2O_3: at 4-coordinated sites, methanol forms from bidentate CO_2 bridged between two sites via formate, while at 3-coordinated sites, CO formation from monodentate CO_2 is favored[115]. Rungtaweevoranit et al.[116] discovered XPS evidence of Zr reduction in the presence of Cu when studying Cu nanoparticles deposited on UiO-66, suggesting an interaction between the Cu NPs and the UiO-66 Zr-node. Similar findings from XPS on CuZn@UiO-67 samples, with 100% bipyridine-type linkers treated with reaction gas, indicated Zr(IV) reduction to Zr(III), likely caused by H adsorption.[117]

These findings, in combination with H_2 and CO_2 TPD results, suggest Zr cluster participation in the reaction via H spillover from Cu and CO_2 adsorption on unsaturated Zr sites.[117] However, when the catalyst was prepared with regular UiO-67, both CH_3OH selectivity and catalytic stability decreased. Importantly, the crystallinity and specific surface area of the MOF were significantly reduced by the deposition of copper, preventing the well-defined MOF structure of UiO-67 during subsequent experiments. These studies show us that high methanol selectivity is attributed to this interface and the crucial role of the Metal Zr-MOF interface.

Similarly, studies on Pt-based CO_2 hydrogenation catalysts, such as the work by Román-Martínez et al., where Pt/C and Pt-M/C (M = Mg, Ca) as CO_2 hydrogenation catalysts are explored.[118] A negative correlation is reported between Pt particle size and turnover frequency for the RWGS reaction over Pt/C. Iglesia and Wei later investigated the reverse methanation reaction, methane reforming to syn gas, over supported Pt catalysts.[119] Their findings indicated that C−H bond breaking was the rate-determining step, with the turnover frequency of methane activation increasing with decreasing Pt particle size. These studies suggested that stabilizing small Pt particles is crucial for developing catalysts for CO_2 hydrogenation, aiming at syngas or methane production.

Combining the two approaches, Pt was incorporated into the UiO-67 Zr-MOF framework by grafting it onto a bipyridine-based linker, and a stable catalyst called UiO-67-Pt was created. This catalyst maintained its well-defined MOF structure even after long-term operation, making it an ideal model system for studying the influence of the MOF framework on the hydrogenation reaction. CO_2 hydrogenation, when performed at high temperatures and pressures using UiO-67-Pt with H_2/CO_2, demonstrated CO_2 hydrogenation activity, resulting in CO and methanol as the primary reaction product and CH_4 as a secondary product formed from CO. In a performance comparison between UiO-67-Pt and Pt/C, Pt/SiO_2, and Pt/Al_2O_3 catalysts, it was found that Pt/C and Pt/SiO_2 produced only CO and did not produce methane and had lower turnover frequency, while Pt/Al_2O_3 produced mainly CO and a modest amount of methane and methanol.

UiO-67-Pt also showed a positive correlation between CO_2 conversion and the degree of Pt reduction, consistent with recent literature. At the same time, CO selectivity remained above 90% under all tested conditions, showcasing the suitability of the partially bipy-functionalized UiO-67 Zr-MOF framework as a support for Pt-catalyzed reverse-water-gas shift reaction by stabilizing Pt metal nanoparticles within framework cavities. UiO-67-Pt also formed substantial amounts of methanol (up to 18% selectivity) and smaller amounts of methane (up to 2% selectivity). UiO-67-Pt was further studied with a focus on elucidating the role of the UiO-67 framework in CO_2 hydrogenation to methanol through kinetic investigations. Operando infrared spectroscopy, steady-state, and transient kinetic studies were also employed for this purpose, which are rarely used in MOF catalysis literature.[120, 121]

When the focus is set on the dynamic role of the Zr-node in UiO-67-Pt during the CO_2 hydrogenation reaction, the influence of the amount of defective open Zr sites on the

formation of all three carbon-containing reaction products: methanol, methane, and CO was investigated. The study showed a positive correlation between the number of node defects and the number of surface intermediates leading to methanol and methane formation. In contrast, the CO formation rate was almost invariant with defect density. These results strongly suggest that the rate-limiting step of CO formation occurs at the Pt NPs, while the rate-limiting step of methane formation, like methanol, takes place at the Pt NP–Zr node interface.

Steady-state and transient water co-feed experiments involving isotope labelling were also employed to gain insight into the role of node hydration and the influence of water in the reaction. Furthermore, water co-feed was found to promote the desorption of methanol, while it is detrimental to methane formation. Experiments involving either dehydrated or pre-hydrated Zr-nodes showed higher methanol and methane formation rates over the dehydrated Zr-node. Transient experiments suggested that the difference is related to competitive adsorption between methanol and water. Adding surplus water to the feed inhibits methane formation but not methanol formation, suggesting that methanol selectivity may be optimized by steam addition to the reactant gas feed. Moreover, transient H_2O co-feed experiments showed that introducing H_2O causes substantial amounts of methanol to desorb from the catalyst while removing H_2O causes re-absorption. No hydrogen transfer from H_2O to the desorbed methanol was also observed.

To further understand the role of water in methanol desorption and explain experimental observations, we developed computational models of a hydrated Zr-node with one missing linker. On this missing linker defect site, we could adsorb and desorb methanol and water and calculate the free energies involved using DFT simulations. In all cases, the computed energy barriers connecting these intermediates are very low, suggesting that thermodynamics mainly dictates the pathway. These DFT calculations were also confirmed using a microkinetic model constructed with all possible methanol and water desorption reaction pathways. The Micro Kinetic Model (MKM) showed that, at equal or larger concentrations of water compared to methanol, the concentration of species containing methoxy groups was very low, consistent with them not being observed under experimental conditions.

As explained above, co-feed experiments showed that adding water into the system initially increases the observed methanol concentration. To gain further insight into this experimental observation, we set up an MKM where different amounts of water are introduced to the system, and these simulations show that when any additional water is introduced into the system, it causes methanol to desorb from the system, in agreement with the experimental observations. To determine the reaction leading to H/D exchange and the relevance of this process, DFT calculations were performed considering deuterated species and different proton-transfer mechanisms.

All mechanisms in this study proceeded without any additional energy barriers beyond thermodynamics, showing that these reactions favor the desorption of CH_3OH. Our calculations have also shown that methanol is more strongly adsorbed to a hydrated node

than a dehydrated node, which could partially account for the larger methanol formation rate at the reaction onset. Structural and electronic analysis of relevant intermediates suggests that the reason for the larger adsorption energies for CH_3OH is the formation of an H-bond between MeOH and the terminal OH.

To evaluate the influence of linker defects on methanol and water adsorption, we built two model systems in which two missing linkers in adjacent and opposite positions were replaced by −OH groups and calculated the methanol adsorption in each model. These energies show that methanol binds stronger on a node with a single missing linker than on nodes with an additional, adjacent, or opposite missing linker defect. In the case of adjacent linkers, the adsorption energies change drastically, strongly suggesting that having a larger number of defects increases the number of active sites to produce methanol and facilitates methanol desorption. These results show that water and missing linkers play an important role in methanol desorption by displacing the equilibria or changing the methanol adsorption energies.

However, we also found that water does not have an important influence on the CH_3OH formation rate at steady state. Instead, it decreases the rate of methane significantly. An explanation for this observation is that the interaction of adsorbed CO with a Zr atom from a node should be feasible at the interface between Pt NPs and Zr nodes. This coordination would increase the electrophilicity of C and favor the hydride transfer, which has been proposed to be the rate-limiting step for the CO hydrogenation to methane with Pt-NPs. When adding water to the system, the equilibria between CO and water will be displaced, favoring water coordination and disfavoring methane formation. In the case of methanol, this competition occurs before forming formate. Therefore, it would not influence the rate-limiting step of methanol, which we propose to be the hydrogenation of formate.

The mechanistic aspects of CO_2 hydrogenation over UiO-67-Pt were also extensively investigated, emphasizing the role of the UiO-67 framework, but this had never been investigated before in the literature. We developed unique computational models that are periodic in nature and represent the edges and terraces of the ~1.6 nm diameter Pt nanoparticles that are grown inside the iO-67 MOF. These models better represent the experimental system as they don't show unreasonably high adsorption energies that are observed in small metal clusters due to geometry and electronic finite size effect, which only vanishes when the platinum clusters are larger than 1.6 nm. Using these models, we found that Pt nanoparticles within the MOF structure facilitate hydrogen activation, forming formate species at the Zr nodes due to the reaction between adsorbed CO_2 and hydrogen spillover from adjacent Pt NPs. Mechanistic insights further revealed that methanol formation was distinct from the production of CO and methane, except for the hydrogen activation process on the Pt NPs. In addition, the data consistently pointed to CO desorption as the rate-limiting step in the reverse water gas shift reaction over UiO-67-Pt while shedding light on the significance of formate species in the reaction pathway. Transient data suggested that the rate-limiting step for methanol formation was the hydrogenation of formate species, with formate species being the most prevalent intermediates.

Combining steady state and transient kinetic methods revealed that methanol is formed from CO_2 via formate intermediates at open Zr-sites at the interface between the Pt NP and the Zr-node. The study further showed that methanol is mechanistically separated from the byproducts, methane and CO, and that methane is formed mainly via CO on this catalyst. The abundance of formate species was constrained by the number of available Zr sites, which were limited due to linker detachment during Pt NP growth during catalyst activation. Moreover, the number of intermediates exceeded the count of open Zr sites in the MOF lattice surrounding each Pt NP, indicating the presence of additional Zr sites for formate formation. This information supports the assertion that methanol primarily forms at the interface between Pt NPs and linker-deficient $Zr_6O_4(OH)_4$ nodes situated on the surface of the Pt NP.

As mentioned above, to understand and explain the mechanistic insights for CO_2 hydrogenation towards methanol, methane, and CO formation from the experiments, we investigated different possible active sites within the UiO-67-Pt MOF by developing five unique computational models. We used these models to compare various possible pathways for CO_2 hydrogenation. We found that a synergistic interaction between defective $Zr_6O_4(OH)_4$ clusters and encapsulated nanoparticles is needed for favoring CO_2 activation. In the cases where node defects are located on Pt-edges, methanol is the preferred product. We show that formate is an intermediate of this reaction, and its hydrogenation is the RDS. Migration of formate over the Zr node is feasible, slowing down its hydrogenation, and hence can be detected experimentally. When node defects are located on a Pt(111) surface, the formation of CO is preferred over formate, and this CO migrates over the Pt surface, favoring its hydrogenation to methane. CO desorption is favored at large CO coverages, and this desorption is the RDS for CO formation. This reactivity model is consistent with the methane formation observed when using pyrolyzed UiO-67 featuring large Pt NPs and is also consistent with the selective formation of methanol over methane in the UiO-67-Pt and pyrolyzed UiO-67 with small Pt NPs characterized by a large number of Pt-edges.

We also successfully correlated the infrared signals corresponding to CO and bidentate formate with platinum nanoparticles and Zr-clusters using the developed models that simulated the interface between the defective Zr-clusters and encapsulated Pt nanoparticles. We demonstrated how CO, methane, and methanol are formed through free energy calculations. These findings help to clarify the experimentally observed absence of methane with smaller nanoparticles and the lower methane and methanol formation rates on MOFs with fewer defects. This correlation has broadened our understanding of the complexity of the reaction mechanism, emphasizing the necessity of understanding both individual components of the catalytic system and their interactions to augment catalytic activity.

To summarize, we use DFT calculations to explain the mechanism for the formation of methanol, methane, and CO, along with their rate-limiting steps; we also show the importance of studying the interfaces of Pt NP and Zr-node of the MOF-67 in these complex catalytic systems. We are able to explain the presence of experimentally observed intermediate products, which show that Pt NPs encapsulated in MOF are multi-component

systems that should be treated by considering multiple models. Our results highlight the difficulties of having selective reactions using heterogeneous catalysts and show that understanding the reaction mechanism allows for tuning the different sites to favor the desired reactions. With this research, we show the importance of computational analysis of reaction mechanisms and catalyst design. As computational capabilities continue to evolve, the capacity to accurately model and predict catalytic behavior will enhance our ability to design catalysts rationally, paving the way for more effective energy storage and conversion strategies.

3 Introduction to theoretical background

In recent years computer simulations have become invaluable for interpreting experimental results and predicting novel chemicals and materials. Over the years, advancements in computational power and algorithms have significantly improved the accuracy of these calculations. As a result, developing algorithms for electronic structure calculations have garnered substantial attention in the field.

This thesis primarily focuses on Density Functional Theory which has emerged as a widely used technique in computational chemistry due to its acceptable accuracy and relatively low computational cost. Using DFT, a wide range of molecular properties can be predicted, including molecular structures, vibrational frequencies, reaction paths, free energies, and kinetics of reaction steps.

3.1 The Schrödinger equation

The aim of quantum calculations is to describe the behaviour of all the electrons in a system, which requires solving the Schrödinger equation[122]. The time-independent Schrödinger equation is given by *eq (1)*.[123]

$$\hat{\mathrm{H}}\psi = E\psi \qquad eq\ (1)$$

Where $\hat{\mathrm{H}}$ is the Hamiltonian operator, ψ is the wavefunction of a quantum mechanical system, and E is the electronic energy of the system. Hamiltonian is partitioned as shown in *eq (2)*.

$$\hat{\mathrm{H}} = \hat{T}_{\mathrm{e}} + \hat{T}_{\mathrm{n}} + \hat{V}_{\mathrm{ne}} + \hat{V}_{\mathrm{nn}} + \hat{V}_{\mathrm{ee}} \qquad eq\ (2)$$

Where terms $\hat{T}_e$ and $\hat{T}_n$ are the kinetic energies of the electron and nucleus, $\hat{V}_{ne}$ and $\hat{V}_{nn}$ are electron-nucleus and nucleus-nucleus interactions, and finally $\hat{V}_{ee}$ explains electron-electron interaction and are defined in *eq (3)* to *eq (7)*.

$$\hat{T}_e = -\frac{1}{2}\sum_{i}^{N}\frac{\nabla^2}{m_i} \qquad eq\ (3)$$

$$\hat{T}_n = -\frac{1}{2}\sum_{A}^{M}\frac{\nabla^2}{M_A} \qquad eq\ (4)$$

$$\hat{V}_{nn} = \sum_{A=1}^{M}\sum_{B>1}^{M}\frac{e^2 Z_A Z_B}{|R_A - R_B|} \qquad eq\ (5)$$

$$\hat{V}_{ee} = \sum_{i=1}^{N}\sum_{j>1}^{N}\frac{e^2}{|r_i - r_j|} \qquad eq\ (6)$$

$$\hat{V}_{ne} = -\sum_{i=1}^{N}\sum_{A=1}^{M}\frac{e^2 Z_A}{|r_i - R_A|} \qquad eq\ (7)$$

Inserting *eqs (3)* to *(7)* into *eq (1)*, the Schrödinger equation can be written as ($\hbar$ = m_e = 1) :

$$\hat{\mathrm{H}}\psi = \left[-\frac{1}{2}\sum_{i=1}^{N}\nabla_i^2 - \frac{1}{2}\sum_{A=1}^{M}\frac{\nabla^2}{M_A} - \sum_{i=1}^{N}\sum_{A=1}^{M}\frac{Z_A}{|r_i - R_A|} + \sum_{i=1}^{N}\sum_{j>1}^{N}\frac{1}{|r_i - r_j|} + \sum_{A=1}^{M}\sum_{B>1}^{M}\frac{Z_A Z_B}{|R_A - R_B|}\right]\psi = E\psi$$

$$eq\ (8)$$

Here, the integers i and j denote the N electrons in the system and A and B the M nuclei. The first and second terms are kinetic energies of electrons and nuclei, the third is nuclei-electron repulsion, and the fourth and fifth are electron-electron and nuclei-electron repulsion. As we have seen here, the Schrödinger equation is a many-body problem that is very difficult to solve directly but can be tackled with approximations[124] explained below.

3.2 Born-Oppenheimer approximation

As seen in the previous section, the Schrödinger equation is a $3N_e$ dimensional partial differential equation, which is impossible to solve analytically. To solve this equation, the first approximation is that nuclei are several orders of magnitude heavier than the electron and can be assumed to be static and due to this enormous mass, the kinetic energy of nuclei is much smaller than the electrons' kinetic energy. Therefore, the kinetic energy term of the nuclei becomes invariant, and the nuclei-nuclei repulsive interaction becomes a constant for each set of nuclear coordinates. These assumptions allow the total wavefunction to be written as the product of electronic and nuclear wavefunction, as shown in *eq (9)*.

$$\psi(r,R) = \psi_n(R)\psi_e(r,R) \qquad eq\ (9)$$

Where $\psi_n(R)$ is the wavefunction describing nuclei, and it only relates to nuclei position R and $\psi_e(r,R)$ is the wavefunction describing the electrons, and finally, the electronic Hamiltonian gets reduced to:

$$\hat{\mathrm{H}}_{ele}\psi = \left[-\frac{1}{2}\sum_{i=1}^{N}\nabla_i^2 - \sum_{i=1}^{N}\sum_{A=1}^{M}\frac{Z_A}{|r_i - R_A|} + \sum_{i=1}^{N}\sum_{j>1}^{N}\frac{1}{|r_i - r_j|}\right]\psi = E_{ele}\psi \qquad eq\ (10)$$

This division of motion of nuclei and electrons into independent mathematical problems is the Born-Oppenheimer approximation, and the total energy for the system becomes:

$$E = E_{ele} + \sum_{A=1}^{M}\sum_{B>1}^{M}\frac{Z_A Z_B}{|R_A - R_B|} \qquad eq\ (11)$$

3.3 Hartree-Fock theory

Born-Oppenheimer approximation makes the Schrödinger equation simpler, but it remains impossible to solve exactly for systems containing many electrons, so more simplifications are needed. Hartree proposed a self-consistent field method in 1928, simplifying the wavefunction description and energy calculation[125]. According to this method, the corresponding single-electron wave function can describe each electron's state, and the total electron states can be obtained by multiplying all single-electron wavefunctions together. In other words, the wavefunction of an n-electron system can be treated as a simplified system of n single electron wavefunction:

$$\psi(r) = \psi_1(r_1).\psi_2(r_2)....\psi_n(r_n) \qquad \textit{eq (12)}$$

From *eq (12)*, it is evident that considering electrons that ignore each other is a large approximation and excludes the antisymmetric principle or the electronic or fermionic spin.

To satisfy the antisymmetric nature of the wavefunction and the Pauli exclusion principle, a Slater determinant[126] is constructed to represent the wavefunction of the N electron system instead of a simple product. With this stater determinant, the exchange of two electrons changes only the sign of the wave function as seen in *eq (13)*, but the probability of finding the electron remains the same.

$$\psi(\vec{x}_1, \vec{x}_2, \dots, \vec{x}_N) = -\psi(\vec{x}_2, \vec{x}_1, \dots, \vec{x}_N) \qquad \textit{eq (13)}$$

$$|\psi(\vec{x}_1, \vec{x}_2, \dots, \vec{x}_N)|^2 = |\psi(\vec{x}_2, \vec{x}_1, \dots, \vec{x}_N)|^2 \qquad \textit{eq (14)}$$

Further simplification is brought on by decoupling the electrons' motion and calculating each electron's energy in the averaged static field V_{eff} through a mean field approximation, meaning that even though each electron moves independently of all the others, it still feels the Coulomb repulsion due to the average positions of all the other electrons in the system. With these approximations, the new Hamiltonian can be written as:

$$\hat{\mathrm{H}} = -\frac{1}{2}\sum_{i=1}^{N} \nabla_i^2 - \sum_{i=1}^{N}\sum_{A=1}^{M} \frac{Z_A}{|r_i - R_A|} + \sum_{i=1}^{N} V_{eff} \qquad \textit{eq (15)}$$

With these approximations in place, the Hartree-Fock method approximates the N-electron wavefunction as a single Slater determinant made of N one-electron wavefunctions. As a result, the Hamiltonian can be expressed as:

$$\hat{\mathrm{H}} = -\frac{1}{2}\nabla_i^2 - \sum_{A=1}^{N} \frac{Z_A}{|r_i - R_A|} + V_i^{HF} \qquad \textit{eq (16)}$$

Here, V_i^{HF} is a two-electron operator representing an electron's average repulsive potential to the other N-1 electrons and can be written as:

$$V_i^{HF}(\vec{x_1}) = \sum_{i}^{N} \left(\hat{J}_i(\vec{x_1}) - \hat{K}_i(\vec{x_1}) \right) \qquad \textit{eq (17)}$$

Where, $(\vec{x_1})$ is the position of the electron, $\hat{J}_i$ is the Coulomb integral, and $\hat{K}_i$ is the Exchange integral given by:

$$\hat{K}_i(\overrightarrow{x_1})\chi_i(\overrightarrow{x_1}) = \int \chi_j^*(\overrightarrow{x_2})\frac{1}{r_{12}}\chi_i(\overrightarrow{x_2})dx_i\chi_i(\overrightarrow{x_1}) \qquad eq\ (18)$$

From *eq (18)*, we see that V_i^{HF} depends on the spin orbitals χ_i and solving these eigenvalue equations would give us the optimal orbital χ_i and the ground state Hartree-Fock energy and wavefunction. This is done by guessing the first set of spin orbitals and obtaining HF potential, and then with this HF potential, new spin orbitals are calculated. This process is repeated until the energy is minimized and the result meets the convergence criteria. This method of minimizing energy and solving equations self consistently is referred to as variational calculation.[127]

Since the HF method is a mean-field approximation and provides an approximate solution to the Schrödinger equation by assuming that the system's wave function can be approximated as a single Slater determinant, it neglects crucial electronic correlation effects, particularly electron-electron correlation, which does not consider the dynamic correlation between the electronic movements. Neglecting electron-electron correlation in the HF method leads to overestimating the electron-electron repulsion energy, resulting in higher total energies than the exact electronic energies. This is known as the correlation energy, representing the difference between the exact energy and the energy obtained from the Hartree-Fock method.

Post-Hartree-Fock methods such as configuration interaction (CI)[128, 129], coupled cluster (CC)[130], or density functional theory (DFT) are often employed to obtain more accurate energies; these methods take into account electron-electron correlation effects and provide improved descriptions of the electronic structure, yielding lower total energies compared to Hartree-Fock.

3.4 Density functional theory

As seen in the previous section, the component in the Hamiltonian characterizing electron-electron interactions is crucial for evaluating the wavefunction accurately. Density functional theory (DFT) was developed as an alternative to the Hartree-Fock method with lower computational costs; DFT provides a method of solving the many-bodied problem without solving the Schrödinger equation with the full Hamiltonian.

DFT does not use the N-body wave functions of the electrons, but the total density of electrons, which is a physical characteristic. It can be traced back to the Thomas-Fermi model, which assumed an approximately uniform distribution of electrons in an atom.[131] However, this model still had errors in the exchange energy and neglects the electron correlation, a principal disadvantage of the Hartree-Fock method. The density functional theory was built on a firm theoretical foundation with the publication of the Hohenberg-Kohn theorems.[132, 133]

Theorem I: There is a unique one-to-one relation between the external potential $V_{ext}(\vec{r})$ and the ground-state electron density $\rho(\vec{r})$.

Corollary: The ground-state expectation value of any observable, such as $\hat{H}$, is a unique functional of the ground-state electron density.[134] This essentially states that the ground-state density[133] holds as much information as ground-state wavefunctions.

Theorem II: The total ground-state energy $E[\rho]$ is a functional of the ground-state density $\rho(\vec{r})$ and is of the form:

$$E[\rho] = F[\rho] + \int \rho(\vec{r}) V_{ext}(\vec{r}) d\vec{r} \qquad \textit{eq (19)}$$

Where $F[\rho]$ is a universal functional for any many-electron system that delivers the system's ground-state energy if and only if the input density is the true ground-state density. $E[\rho]$ is variational in that it is minimized by the ground-state density corresponding to V_{ext}.

Corollary II: The functional $F[\rho]$ is independent of any information about the nuclei and is universal for any many-electron system.

These two theorems tell us that the ground-state density uniquely defines the potential of any system, and the minimum ground-state energy corresponds to the ground-state density. So, if the functional $F[\rho]$, which connects the system's electron density with its energy, is known, we can determine the ground state energy and density by minimizing $E[\rho]$. We only need to solve for the density, ρ since the density holds as much information as the wavefunction. An explicit expression for universal functional $F[\rho]$ is not known. However, Kohn and Sham provided a method for finding the ground-state density[135].

3.4.1 Kohn-Sham equations

Schrödinger equation can be solved using the method proposed by Kohn and Sham where replaced the interactive system with a non-interactive one, assuming the electronic ground states are the same in both. This mapping decouples the electron-electron interactions in all but one Hamiltonian term, simplifying calculations and still theoretically producing the exact ground-state density and the total energy can be written as:

$$E[\rho] = T[\rho] + V_{ee}[\rho] + E_{xc}[\rho] + \int V_{ext}(r)\rho(r)d^3r \qquad \textit{eq (20)}$$

Where $T[\rho]$ is the kinetic energy of the non-interactive electrons, $V_{ee}[\rho]$ is the classical Coulomb electron-electron interaction term, $E_{xc}[\rho]$ is the exchange-correlation term, and the final integral term is the interaction of electrons with the external potential created by the nuclei. The first two terms in *eq (20)* are known exactly, and the exchange-correlation term

contains the Coulomb functional, the Exchange functional, the Correlation functional and the Kinetic functional and must be approximated.

Kohn–Sham equations can be solved iteratively given that:

$$\widehat{H_{KS}}[\rho] = \widehat{T_0} + \widehat{V_H} + \widehat{V_{xc}} + \widehat{V_{ext}} \qquad \textit{eq (21)}$$

$$\rho(\vec{r}) = \sum_{i}^{N} |\varphi_i(\vec{r})|^r \qquad \textit{eq (22)}$$

$$\widehat{H_{KS}}\varphi_i = \epsilon_i \varphi_i \qquad \textit{eq (23)}$$

An initial guess for the density ρ_0 is made and put into *eq (21)*, giving us the Hamiltonian $\widehat{H_{KS}}$ used in *eq (23)* to generate a set of φ_i, which is further used in *eq (22)* to give us a new density ρ_1. This is repeated iteratively until a self-consistent density is found giving us the ground state electron density, which can further be used to calculate the total energy.

3.5 Exchange–correlation functional

Up to this point, the Kohn-Sham approach demonstrates that the ground-state energy can be evaluated by finding a self-consistent solution to a set of single-particle equations, given that the Kohn-Sham approach is exact except for the exchange-correlation functional $E_{xc}[\rho]$. The natural form of the exchange-correlation functional is unknown and must be approximated to calculate anything in practice.

A large number of functionals have been developed to approximate $E_{xc}[\rho]$. However, every one of these functionals can be written in the same general form:

$$E_{xc}[\rho(\vec{r})] = \int \rho(\vec{r})\varepsilon_{xc}(\vec{r})\overrightarrow{dr} \qquad \textit{eq (24)}$$

This means that functionals can be characterized by how they sample the density around each electron to construct the exchange-correlation energy density $\varepsilon_{xc}(\vec{r})$. The simplest approximation of them is to assume that the density behaves locally and is homogeneous everywhere, and this is referred to as local density approximation (LDA)[136-138] and is given by:

$$E_{xc}^{LDA}[\rho(\vec{r})] = \int \rho(\vec{r})\varepsilon_{xc}^{hom}(\vec{r})\overrightarrow{dr} \qquad eq\ (25)$$

Where, $\varepsilon_{xc}^{hom}(\vec{r})$ is the exchange-correlation energy per particle of a homogeneous electron gas of charge density ρ. The exchange term has been found analytically and is a reasonable starting guess. Although LDA performs reasonably well for systems with slowly varying density, like estimating the properties of bulk materials, where the valence electron density changes slowly and resembles the homogenous electron gas. However, when density varies rapidly in systems such as isolated molecules, it gives a poor approximation for energetic details, such as overestimated binding energies, energy barriers, etc.

The Generalized Gradient Approximation (GGA) method is an improvement to the LDA method, addressing its shortcomings. To rectify this, GGA incorporates the density gradient in the exchange-correlation functional to better reflect the non-homogeneity of the actual electron density. In doing so, the GGA method considers the system as a non-uniform electron gas and incorporates non-local electron effects into the functional, offering a more accurate representation of the system. The general form of GGA functional can be written as[139]:

$$E_{xc}^{GGA}[\rho(\vec{r})] = \int \rho(\vec{r})\varepsilon_{xc}^{hom}[\rho(\vec{r})]F_{xc}[\rho(\vec{r}), \nabla\rho(\vec{r})]\overrightarrow{dr} \qquad eq\ (26)$$

where the F_{xc} function is called an enhancement factor and can be divided into F_x and F_c. The most popular GGA functional was developed by Perdew, Burke, and Ernzerhof and is known as PBE[140]. This functional is most commonly applied to molecules and solids, including metals, but they fail to accurately predict the electronic properties of some systems, particularly highly correlated systems. However, PBE performs well for a wide variety of systems and is probably the most broadly used functional and used in this thesis work.

Previously introduced functionals suffer from electronic self-interaction, as the exchange parts of the functionals are poorly described. However, the exchange part is well-defined for Hartree-Fock but does not account for correlation. Becke proposed using a portion of the exact (non-local) HF exchange energy and combine with conventional GGA as a local or semi-local exchange-correlation functional.[141, 142] The general form for hybrid functionals is given by:

$$E_{xc}^{Hyb}[\rho] = E_{xc}^{GGA}[\rho] + \alpha\,[E_x^{HF}[\emptyset_{sel}] - E_x^{GGA}[\rho_{sel}]] \qquad eq\ (27)$$

The parameter α is a semi-empirical constant determined by fitting experimental data, $\emptyset_{sel}$ are the selected orbitals to which the exact exchange is applied (correlated d electrons), and $\rho_{sel}$is the density of the selected electrons. One well-known and widely used hybrid functional is the B3LYP, which combines 20% Hartree-Fock exchange with an 80% DFT exchange-correlation[143]. Hybrid functionals generally offer improved accuracy compared to

pure DFT functionals but at a higher computational cost. They are beneficial when studying systems where accurate descriptions of weak and strong interactions are crucial.

3.6 Basis set

The Kohn-Sham equations give us an overview of a system of many electrons, and it can successfully model simple systems with many electrons in a finite space. To solve the single-particle Kohn-Sham equations, the single-electron wavefunctions must be expanded based on a basis, and a finite basis set is essential to describe infinite large-scale space, represented by the composition of numerous repeated periodical unitcell in three-dimensional space. This transforms the series of single-particle Schrödinger equations into a matrix equation that can be solved computationally.

The orbitals are formally defined over all space but, in practice, are localized around atoms. To calculate Kohn-Sham orbitals and calculate ground state properties of the system using DFT[135], the electron density must be represented using some basis set. A basis set is a set of functions representing the electronic wavefunction in the Hartree-Fock method or density functional theory. The basis set consists of either atomic orbital or plane waves.

3.6.1 Atom-Centred basis sets

Atomic orbital basis sets offer a simple, intuitive way to solve the equations of DFT. Atomic or molecular orbitals can be created using atom-localized basis functions. They are usually derived from solutions to the Schrödinger equation for an isolated atom. However, this is not possible in the case of molecules, so the orbitals are expanded in some known basis functions, as shown here:

$$\psi_i(r) = \sum_{\mu=1}^{K} c_{i\mu}\phi_\mu(r) \qquad eq\ (28)$$

Here K is the number of basis functions used to generate K number of orbitals. There are two types of Atom-centred orbitals: Slater-type orbitals (STOs)[144] and Gaussian-type orbitals (GTOs).[145, 146] However, Gaussian orbitals are often used to facilitate the computation of integrals and are discussed here.

GTOs are expressed in the following form:

$$\phi = Ne^{-\alpha r^2} \qquad eq\ (29)$$

Here N is the normalization factor, and α is a free parameter. Usually, Slater-type functions have a shape that matches the shape of typical orbital functions. They also feature a cusp at r = 0 and show exponential decay for larger r values. In contrast, the GTOs do not show a cusp at r = 0 as they have zero slope and decay rapidly for larger r values than Slater functions. Even though Slater-type functions are better for describing orbitals than Gaussian functions, evaluating the integrals over the Slater function takes longer than evaluating Gaussian functions.

Since the product of two GTOs is a third one situated between them, which is not the case for STOs. This property avoids the problem of handling the two-electron integrals involving four different centres, which is computationally expensive. Instead, an STO can be approximated by combining several GTOs, which is usually more efficient than using STOs directly. Those are called contracted Gaussian functions (CGF) and describe the complexity or precision with which each atomic orbital is defined.

Gaussian basis sets often do not accurately describe electron density near the nucleus, and the accuracy of the calculation depends greatly on the basis set's completeness; an infinite basis set is needed to reach the exact wavefunction or electronic density, which would be impossible to solve computationally. Usually, double-zeta and triple-zeta basis sets give reasonable precision and description of the system. Another drawback of the Gaussian basis is that the localized nature of such basis sets results in a basis set superposition error (BSSE) in areas where basis functions overlap.

3.6.2 Plane Wave basis sets

As the name suggests, these are constructed from plane waves, and the wavefunction is represented as a linear combination of plane waves and is generally used for calculations involving periodic systems. In a plane wave basis set, the wavefunctions are expanded as a Fourier Series, and the coefficients of the series are stored in a regular grid up to a maximum wave vector called the plane wave cut-off. This is done by using Bloch's theorem[147], which states that eigenfunctions of the Schrödinger equation with a periodic potential are given by:

$$\psi_{nk} = u_{n,k} e^{ik.r} \qquad \textit{eq (30)}$$

$$\psi_{nk}^{m}(r) = \sum_{G} c_{(k+G)}^{m} \, e^{[i(k+G).r]} \qquad \textit{eq (31)}$$

where $u_{n,k}$ gives the periodicity of the lattice, and like any periodic function, the Bloch function $u_{n,k}$ can be expanded using a Fourier series of terms that are the reciprocal lattice vectors. *eq (30)* gives the eigenfunctions of the wave equation with a periodic potential, and *eq (31)* shows that each eigenfunction of the KS equations for a periodic system that can be

spanned by a discrete set of plane-waves with wave vectors $K + G$ are characterized by a principal quantum number n and a crystal momentum k.

Using Bloch's theorem, the problem of the infinite number of electrons has now been defined by an infinite number of reciprocal space vectors within the first Brillouin zone of the periodic cell, k. The kinetic energy in the Hamiltonian is diagonal, but the plane waves are orthogonal. Therefore, as a good approximation, the expansion must be truncated at a certain cut-off that is given by:

$$|k + G|^2 \frac{\hbar^2}{2m_e} < E_{Cut} \qquad eq\ (32)$$

The effect of the cut-off is to produce a less accurate wavefunction and hence produce higher energy of the system. As seen till now, these basis sets are not dependent on the atomic coordinates of nuclei in the system and are well-suited for describing periodic systems. Here Kinetic Energy, Hartree Energy and external Potential Energy are typically computed in Fourier space, using fast Fourier transforms, to move between real space and k-space, making some operations faster. While the periodic and unlocalized nature of plane wave basis sets helps avoid superposition error, one major drawback is that the empty regions of the simulation are described with the same accuracy as areas that contain atoms and increase computational cost.

3.6.3 Pseudopotentials

In the plane-waves method, the core electrons need a very large plane-wave basis set to be correctly modelled because the electrons' wavefunctions oscillate near the core because of strong ionic potential. But, most physical and chemical properties of solids depend on the valence electrons and less on the core electrons. Therefore, we can use pseudopotential approximation to reduce the size of the plane wave basis set by replacing core electrons with approximated potentials and considering these electrons and the nuclei together as rigid non-polarisable ionic cores.[148]

The pseudopotential approach reduces the electrons needed for the calculations and reduces the computational cost,[149] as there are fewer Kohn-Sham eigenstates to compute. In addition, creating a pseudopotential that has the same effect on the valence electron wavefunctions away from the core, but is smooth in the core region, dramatically reduces the number of plane waves needed to represent those wavefunctions.

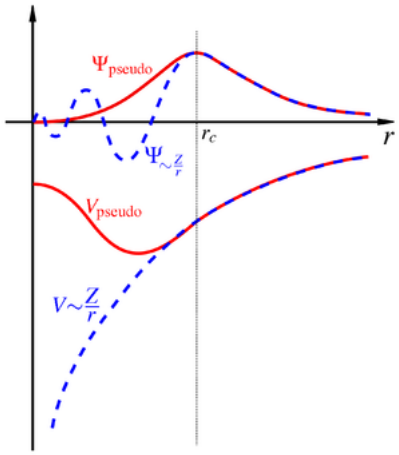

Figure 11: Shows the real wavefunction (dashed blue line) and pseudopotential wavefunction (solid red line) and their potential and pseudopotential, respectively. The r_c represents the dividing line, after which the real all-electron and pseudo-electron potentials coincide. (Source: https://en.wikipedia.org/wiki/ Pseudopotential)

There are two different types of pseudopotentials. High-cutoff-energy required pseudopotentials are referred to as "hard," whereas low-cutoff-energy required pseudopotentials are referred to as "soft."[150] This thesis treats the valence electrons explicitly within the GTH (Goedecker-Tetter-Hutter) pseudopotentials as part of the CP2K code used for all the DFT calculations involved.

3.6.4 Gaussian and plane waves (GPW) method

This dual basis approach uses both Gaussian and plane waves types of basis sets simultaneously to solve the Kohn-Sham equations, where atom-centred Gaussian basis functions represent the single-particle wave functions and an auxiliary basis of Plane Waves is used for expanding the electronic density with the density represented through plane waves on a regular grid, Fast Fourier Transform (FFT) can be used to solve the Poisson equations efficiently and to obtain the Hartree energy. The choice to use Gaussian or plane waves for each term depends on which basis has greater numerical efficiency.[151, 152]

3.7 Dispersion correction

A well-known challenge for density functional theory is accounting for dispersion interactions resulting from fluctuating charge distributions, generating instantaneous multipoles that are proportional with $\sim \frac{1}{r^6}$. In both HF and DFT methods, the inclusion of long-range electron correlation effects is missing, and a semi-local functional cannot describe such long-range interactions where the electron clouds barely overlap. However, adding an

extra energy term can account for these dispersion interactions or van der Waals forces.[153] Many corrections have been developed to overcome this issue, ranging from semi-empirical corrections to non-local long-range density functionals. The Grimme corrections are one such example of a semi-empirical method that is popular and employed in the simulations carried out for this thesis.[154]

As described above, van der Waals's force arises from the motion of electrons, leading to multipoles' generation. In the Grimme method, the dispersion energy term is added to the Kohn-Sham energy, and it does not depend on electron densities but only on atomic coordinates. The dispersion energy term is given by:

$$E_{disp}^{DFT-D} = -\sum_{i=1}^{N_{atoms}-1}\sum_{j=i+1}^{N_{atoms}} S_6 \frac{C_6^{ij}}{R_{ij}^6} f_{damp}(R_{ij}) \qquad eq\,(33)$$

Where C_6^{ij} represents the dispersion coefficient for atoms *i* and *j*, located at a distance R_{ij} and S_6 represents a global scaling term uniquely optimized for each DFT functional depending on the repulsive behaviour of the functional used and f_{damp} is a damping function. This thesis uses Becke–Johnson damping version of DFT-D3[155], which is given by:

$$E_{disp}^{DFT-D3(BJ)} = -\frac{1}{2}\sum_{i\neq j}\sum_{n=6,8} S_6 \frac{C_n^{AB}}{R_{AB}^n + \left[f_{damp}^{DFT-D3(BJ)}(R_{BJ}^{AB})\right]^n} \qquad eq\,(34)$$

$$f_{damp}^{DFT-D3(BJ)}\left(R_{BJ}^{AB}\right) = a_1\left(R_{BJ}^{AB}\right) + a_2 \qquad eq\,(35)$$

where a_1 and a_2 are functional-dependent parameters. In this method s_6 is generally fixed to unity and s_8 is optimized for each functional. DFT-D3(BJ) generally outperforms the original DFT-D3(0) version.[155]

3.8 Free energy and thermodynamic corrections

DFT-obtained electronic energies are calculated at 0 K temperature and 0 atm pressure. Thermodynamic corrections are needed to compare energies obtained from calculation with experimental data, and the Gibbs free energies can be given by:

$$G^0 = E_{DFT} + E_{ZPE} + U^0 - TS^0 \qquad eq\,(36)$$

Where, E_{DFT} is the ground-state energy calculated with DFT and E_{ZPE} is the zero-point energy correction and is expressed as:

$$E_{ZPE} = \sum_i \frac{h\mathrm{n}_i}{2} \qquad eq\ (37)$$

The standard molar vibrational, thermal energy is expressed as:

$$U_{vib}^0 = RT \sum_i \frac{h\mathrm{n}_i/k_B}{e^{h\mathrm{n}_i/k_B T} - 1} \qquad eq\ (38)$$

Finally, vibrational entropy is given by:

$$S_{vib}^0 = R \sum_i [\frac{h\mathrm{n}_i/k_B}{e^{h\mathrm{n}_i/k_B T} - 1} - \ln\left(1 - e^{h\mathrm{n}_i/k_B T}\right)] \qquad eq\ (39)$$

Where h is Plank's constant, n_i is the vibrational frequency calculated based on the harmonic oscillator approximation, R represents the gas constant and k_B is Boltzmann's constant.

3.9 Nudged Elastic Band

The Transition state theory is crucial in studying chemical reactions, especially when identifying the highest potential energy maximum along the minimum energy path (MEP), a structure referred to as the transition state. This saddle point gives the energy barrier of the process. For example, a low barrier allows the reactants' thermal energy to overcome it easily, leading to faster reactions. Conversely, a high barrier results in fewer reactants with enough energy to overcome it, slowing the reaction. The nudged elastic band (NEB) method is a computational approach to finding the MEP and the transition state between known initial and final geometries.[156, 157]

The NEB method is widely used for estimating transition rates within the harmonic transition state theory approximation. The NEB method functions by constructing a set of images of the system between the initial and final state. These images are connected via a spring with a spring constant *k* in an additional dimension in the phase space, emulating an elastic band. The band is then optimized by minimizing the force acting on the images, thus directing the band towards the MEP. The following equations represent the force applied to these images:

$$\vec{F_i} = -\vec{\nabla} V(\vec{R_i}) + \vec{F}_i^{spring} \qquad eq\ (40)$$

And

$$\vec{F}_i^{spring} = k_{i+1}\left(\overrightarrow{R_{\iota+1}} - \overrightarrow{R_\iota}\right) - k_i\left(\overrightarrow{R_\iota} - \overrightarrow{R_{\iota-1}}\right) \qquad \textit{eq (41)}$$

Without the proper force projection scheme, the band may be prevented from following a curved MEP due to "corner-cutting". The true force along the path could cause the images to shift away from high-energy regions towards the minima, reducing the density of images where they are most needed. This corner-cutting problem is overcome in the NEB method by ensuring that the spring forces do not interfere with the elastic band's convergence to the MEP and that the true force does not affect the distribution of images along the MEP. This requires estimating the tangent to the path at each image and at every iteration during the minimization. The force components parallel and perpendicular to the path are decomposed, with only the perpendicular component of the true force and the parallel component of the spring force included. The force acting on the images now is given by:

$$\vec{F}_i^{0} = -\vec{\nabla}V\left(\overrightarrow{R_\iota}\right)|_\perp + \vec{F}_i^{spring}.\hat{\tau}_\parallel\hat{\tau}_\parallel \qquad \textit{eq (42)}$$

Where $\hat{\tau}_\parallel$ is the unit tangent vector parallel to the path. This force projection, called "nudging", ensures that the spring forces control the images' spacing along the band. It decouples the dynamics of the path from the distribution of images chosen in the discrete representation of the path. As a result, the spring force does not interfere with the images' relaxation perpendicular to the path, and the relaxed configuration of the images is such that they lie on the MEP and is given by:

$$\vec{\nabla}V\left(\overrightarrow{R_\iota}\right)|_\perp = 0 \qquad \textit{eq (43)}$$

Also, since the spring force only affects the distribution of the images within the path, the choice of the spring constant can be arbitrary. This separation of path relaxation and discrete path representation is crucial for MEP convergence.

4 Summary of articles

4.1 Article I

Influence of Defects and H_2O on the Hydrogenation of CO_2 to Methanol over Pt Nanoparticles in UiO-67 Metal−Organic Framework.

Journal of the American Chemical Society, 142(40), 17105-17118.

In catalysts for CO_2 hydrogenation, the interface between metal nanoparticles (NPs) and the support material is crucial for activity and reaction selectivity. In this study, we investigate the dynamic role of the Zr-node and the influence of H_2O on the CO_2 hydrogenation reaction through steady-state and transient isotope exchange experiments, H_2O co-feed measurements, and DFT calculations. A UiO-67-Pt MOF catalyst was designed with fewer defects to influence the rate of methanol formation, and when compared against a MOF with a higher number of defects, it was revealed that increased Zr-node defects increase methanol and methane formation rates. This result suggests that the methanol and methane formation rates had a similar dependency on Zr node defects, while the CO formation rate was not dependent on defect density. These results strongly suggest that the rate-limiting step of CO formation occurs at the Pt NPs, while methane and methanol formation occurs at the Pt NP−Zr node interface.

By comparing the onset of reaction over a sample with dehydrated Zr-nodes to the onset over a prehydrated sample, it was found that the rate of methanol and methane formation are both higher over a dehydrated node than over a hydrated node. However, adding extra water to the feed inhibits methane formation but not methanol formation, suggesting that methanol selectivity may be optimized by steam addition to the reactant gas feed. Moreover, transient H_2O co-feed experiments showed that introducing H_2O causes substantial amounts of methanol to desorb from the catalyst while removing H_2O causes readsorption. Transient experiments were conducted where no hydrogen transfer from H_2O to the desorbed methanol was observed, suggesting that this difference is related to competitive adsorption between methanol and water. DFT calculations and microkinetic modelling support this conclusion and give further insight into the equilibria involved in the competitive adsorption process. DFT calculations also showed that methanol is adsorbed weakly on less hydrated and more defective nodes, in agreement with experiments, which can contribute to observing larger amounts of methanol with these systems.

4.2 Article II

Mechanistic insights for Hydrogenation of CO2 to Methanol, Methane and CO over Pt Nanoparticles in UiO-67 Metal-Organic Frameworks.

ACS Catalysis 14 (2023): 382-394.

Metal nanoparticles (NPs) encapsulated within Zr-based UiO-67 metal–organic frameworks (MOFs) have increased selectivity toward methanol in CO_2 reduction reactions. However, the reduction mechanism in these systems remains unclear. We built upon prior work examining the synergistic interaction between Pt nanoparticles and $Zr_6O_4(OH)_4$ clusters in UiO-67 and developed five distinct models representing the possible active sites in the Pt ⊂ MOF system.

Density functional theory (DFT) calculations were employed to elucidate the CO_2 reduction mechanism toward methanol, methane, and CO formation. Our findings support previous evidence showing that the interface between the $Zr_6O_4(OH)_4$ cluster and platinum nanoparticles plays a crucial role in the activation of CO_2 to CO or formate intermediates and its further reduction to methane and methanol, respectively. Furthermore, we found different CO_2 hydrogenation mechanisms for interfaces involving Pt-flat terraces and Pt-edges. On Pt terraces and interfaces near Pt terraces, the reaction goes via CO, which can be desorbed as CO(g) or be further reduced to methane. On interfaces near Pt-edges, the reaction proceeds via formate and preferably forms methanol over methane. We designed experiments to validate our computational insights involving large and small Pt nanoparticles interacting with $Zr_6O_4(OH)_4$ clusters. These experiments showed that only CO and methanol were formed when smaller nanoparticles were present. Notably, methane formed with CO and methanol in the presence of larger nanoparticles, highlighting the need for flat platinum surfaces at the interfaces for methane formation. We could also associate the IR signals corresponding to CO and bidentate formate with platinum nanoparticles and $Zr_6O_4(OH)_4$ clusters, respectively. Theoretical models and experimental data provided us with insights into the complexity of the reaction mechanism and emphasized the significance of understanding both the individual components of the catalytic system and their interactions in enhancing catalytic activity..

5 Conclusion and Outlook

This dissertation presents a comprehensive study focused on understanding the mechanism of CO_2RR over a UiO-67-Pt Metal-Organic Framework catalyst. In collaboration with experiments, this theoretical work provides insights into the role of different components of the MOF system, their synergistic interactions, and their influences on the CO_2RR. The research objectives and questions we presented at the beginning of this thesis are answered in the research articles we published as a part of this thesis and are summarized here:

Research objectives:

1. We found that when a defective node forms an interface with the Pt(111) surface, the formation of CO is preferred over formate, and this CO migrates over the Pt surface, favoring its hydrogenation to methane. However, formate is preferred when the defective node forms an interface with a Pt edge formation, which is further hydrogenated to form CH_3OH. This mechanism is consistent with the methane formation observed when using pyrolyzed UiO-67 featuring large Pt NPs and is also consistent with the selective formation of methanol over methane in the UiO-67-Pt and pyrolyzed UiO-67 with small Pt NPs characterized by a large number of Pt-edges.

2. Our calculations show that formate is an intermediate for methanol formation, and its hydrogenation is the RDS. The study further showed that methanol is mechanistically separated from methane and CO and that methane is formed mainly via CO on this catalyst with hydrogenation of CH_3 as RDS. We also find that CO desorption is favored at large CO coverages, and this desorption is the RDS for CO formation.

Research questions:

1. Our calculations show that methanol binds stronger on a node with a single missing linker than on nodes with an additional, adjacent, or opposite missing linker defect. In the case of adjacent linkers, the adsorption energies change drastically, strongly suggesting that having a larger number of defects increases the number of active sites to produce methanol and facilitates methanol desorption.

2. Our calculations show that CO observed in the experiments is from two sources: one that forms on the Pt NPs and some forms at the interface between the Zr node and Pt NPs and migrates onto the Pt surfaces before desorption, suggesting that CO formation is independent of defect density.

3. Using the models we built for DFT calculations, we developed a microkinetic model that shows that methanol is more strongly adsorbed to a hydrated node than a dehydrated node, which could partially account for the larger methanol formation rate at the reaction onset. Structural and electronic analysis of relevant intermediates suggests that the reason for the larger adsorption energies for CH_3OH is the formation of an H-bond between MeOH and the terminal OH.

4. We found that water does not significantly influence the CH_3OH formation rate at a steady state but decreases the methane formation rate. An explanation for this observation is that the interaction of adsorbed CO with a Zr atom from a node should be feasible at the interface between Pt NPs and Zr nodes. This coordination would increase the electrophilicity of C and favor the hydride transfer, which has been proposed to be the rate-limiting step for the CO hydrogenation to methane with Pt-NPs. When adding water to the system, the equilibria between CO and water will be displaced, favoring water coordination and disfavoring methane formation.

5. Using the models that simulate the interface between the defective Zr-clusters and encapsulated Pt nanoparticles, we successfully correlated the infrared signals corresponding to CO and bidentate formate with platinum nanoparticles and Zr-clusters. Experimentally observed CO signal was replicated with DFT calculations on Pt-55 NP at high CO coverages, which is also supported by high desorption-free energies of CO at low coverages. In the case of the formate signal, the observed signal was from the formate intermediate, whose hydrogenation is RDS for methanol formation, and on the formate linker analogs used in the DFT models, suggesting that formate could migrate before hydrogenation.

This work highlights the central role of the synergistic interaction between the defective Zr-clusters and Pt NPs in the successful hydrogenation process and substantially contributes to understanding the CO_2 reduction mechanism in Pt-NP ⊂ UiO-67 systems. Moreover, they provide a framework for designing more efficient catalysts for CO_2 reduction and for producing valuable chemicals such as methane and methanol. Future research could explore other stable and versatile MOF systems containing different metal nanoparticles with varying sizes for CO_2 reduction or substitute Pt NP in UiO-67 with other metal NPs in varying sizes and also aim to develop better computational models to simulate larger catalytic systems, enabling a more detailed understanding of the complex interactions in these systems.

References

1. Wang, J.; Huang, L.; Yang, R.; Zhang, Z.; Wu, J.; Gao, Y.; Wang, Q.; O'Hare, D.; Zhong, Z., Recent advances in solid sorbents for CO 2 capture and new development trends. *Energy & Environmental Science* **2014,** *7* (11), 3478-3518.
2. LINDSEY, R. Climate Change: Atmospheric Carbon Dioxide. https://www.climate.gov/news-features/understanding-climate/climate-change-atmospheric-carbon-dioxide.
3. Meinshausen, M.; Meinshausen, N.; Hare, W.; Raper, S. C.; Frieler, K.; Knutti, R.; Frame, D. J.; Allen, M. R., Greenhouse-gas emission targets for limiting global warming to 2 C. *Nature* **2009,** *458* (7242), 1158-1162.
4. Rosado, H. R. a. M. R. a. P. Energy. https://ourworldindata.org/energy.
5. Kumar, A.; Madden, D. G.; Lusi, M.; Chen, K. J.; Daniels, E. A.; Curtin, T.; Perry IV, J. J.; Zaworotko, M. J., Direct air capture of CO2 by physisorbent materials. *Angewandte Chemie International Edition* **2015,** *54* (48), 14372-14377.
6. McQueen, N.; Gomes, K. V.; McCormick, C.; Blumanthal, K.; Pisciotta, M.; Wilcox, J., A review of direct air capture (DAC): scaling up commercial technologies and innovating for the future. *Progress in Energy* **2021,** *3* (3), 032001.
7. Choi, S.; Drese, J. H.; Eisenberger, P. M.; Jones, C. W., Application of amine-tethered solid sorbents for direct CO2 capture from the ambient air. *Environmental science & technology* **2011,** *45* (6), 2420-2427.
8. Fasihi, M.; Efimova, O.; Breyer, C., Techno-economic assessment of CO2 direct air capture plants. *Journal of cleaner production* **2019,** *224*, 957-980.
9. Fujikawa, S.; Selyanchyn, R.; Kunitake, T., A new strategy for membrane-based direct air capture. *Polymer Journal* **2021,** *53* (1), 111-119.
10. Vergragt, P. J.; Markusson, N.; Karlsson, H., Carbon capture and storage, bio-energy with carbon capture and storage, and the escape from the fossil-fuel lock-in. *Global Environmental Change* **2011,** *21* (2), 282-292.
11. Holm-Nielsen, J. B.; Ehimen, E. A., *Biomass supply chains for bioenergy and biorefining*. Woodhead Publishing: 2016.
12. Burns, W.; Nicholson, S., Bioenergy and carbon capture with storage (BECCS): the prospects and challenges of an emerging climate policy response. *Journal of Environmental Studies and Sciences* **2017,** *7*, 527-534.

13. Almena, A.; Thornley, P.; Chong, K.; Röder, M., Carbon dioxide removal potential from decentralised bioenergy with carbon capture and storage (BECCS) and the relevance of operational choices. *Biomass and Bioenergy* **2022,** *159*, 106406.
14. Snæbjörnsdóttir, S. Ó.; Sigfússon, B.; Marieni, C.; Goldberg, D.; Gislason, S. R.; Oelkers, E. H., Carbon dioxide storage through mineral carbonation. *Nature Reviews Earth & Environment* **2020,** *1* (2), 90-102.
15. Bai, M.; Zhang, Z.; Fu, X., A review on well integrity issues for CO2 geological storage and enhanced gas recovery. *Renewable and Sustainable Energy Reviews* **2016,** *59*, 920-926.
16. Yadav, S.; Mehra, A., A review on ex situ mineral carbonation. *Environmental Science and Pollution Research* **2021,** *28*, 12202-12231.
17. Sanna, A.; Uibu, M.; Caramanna, G.; Kuusik, R.; Maroto-Valer, M., A review of mineral carbonation technologies to sequester CO 2. *Chemical Society Reviews* **2014,** *43* (23), 8049-8080.
18. Veetil, S.; Hitch, M., Recent developments and challenges of aqueous mineral carbonation: a review. *International Journal of Environmental Science and Technology* **2020,** *17*, 4359-4380.
19. White, J. A.; Foxall, W., Assessing induced seismicity risk at CO2 storage projects: Recent progress and remaining challenges. *International Journal of Greenhouse Gas Control* **2016,** *49*, 413-424.
20. Poon, K. C.; Wan, W. Y.; Su, H.; Sato, H., A review on recent advances in the electrochemical reduction of CO 2 to CO with nano-electrocatalysts. *RSC advances* **2022,** *12* (35), 22703-22721.
21. Pei, Y.; Zhong, H.; Jin, F., A brief review of electrocatalytic reduction of CO2—Materials, reaction conditions, and devices. *Energy Science & Engineering* **2021,** *9* (7), 1012-1032.
22. Nitopi, S.; Bertheussen, E.; Scott, S. B.; Liu, X.; Engstfeld, A. K.; Horch, S.; Seger, B.; Stephens, I. E.; Chan, K.; Hahn, C., Progress and perspectives of electrochemical CO2 reduction on copper in aqueous electrolyte. *Chemical reviews* **2019,** *119* (12), 7610-7672.
23. John-Paul, J.; Surya, P., OGA. *Israel Journal of Chemistry* **2014,** *54*, 1451-1466.
24. Xue, Y.; Guo, Y.; Cui, H.; Zhou, Z., Catalyst design for electrochemical reduction of CO2 to multicarbon products. *Small Methods* **2021,** *5* (10), 2100736.
25. Saha, P.; Amanullah, S.; Dey, A., Selectivity in electrochemical CO2 reduction. *Accounts of Chemical Research* **2022,** *55* (2), 134-144.
26. Grammatico, D.; Bagnall, A. J.; Riccardi, L.; Fontecave, M.; Su, B. L.; Billon, L., Heterogenised molecular catalysts for sustainable electrochemical CO2 reduction. *Angewandte Chemie International Edition* **2022,** *61* (38), e202206399.

27. González-Castaño, M.; Dorneanu, B.; Arellano-García, H., The reverse water gas shift reaction: a process systems engineering perspective. *Reaction Chemistry & Engineering* **2021,** *6* (6), 954-976.
28. Anderson, R. B., Fischer-Tropsch Synthesis. **1984**.
29. Porosoff, M. D.; Yan, B.; Chen, J. G., Catalytic reduction of CO 2 by H 2 for synthesis of CO, methanol and hydrocarbons: challenges and opportunities. *Energy & Environmental Science* **2016,** *9* (1), 62-73.
30. Kattel, S.; Liu, P.; Chen, J. G., Tuning selectivity of CO2 hydrogenation reactions at the metal/oxide interface. *Journal of the American Chemical Society* **2017,** *139* (29), 9739-9754.
31. Li, X.; Yang, X.; Zhang, J.; Huang, Y.; Liu, B., In situ/operando techniques for characterization of single-atom catalysts. *Acs Catalysis* **2019,** *9* (3), 2521-2531.
32. Boot-Handford, M. E.; Abanades, J. C.; Anthony, E. J.; Blunt, M. J.; Brandani, S.; Mac Dowell, N.; Fernández, J. R.; Ferrari, M.-C.; Gross, R.; Hallett, J. P., Carbon capture and storage update. *Energy & Environmental Science* **2014,** *7* (1), 130-189.
33. Du, Q.; Rao, R.; Bi, F.; Yang, Y.; Zhang, W.; Yang, Y.; Liu, N.; Zhang, X., Preparation of modified zirconium-based metal-organic frameworks (Zr-MOFs) supported metals and recent application in environment: a review and perspectives. *Surfaces and Interfaces* **2022,** *28*, 101647.
34. Mueller, U.; Schubert, M.; Teich, F.; Puetter, H.; Schierle-Arndt, K.; Pastre, J., Metal–organic frameworks—prospective industrial applications. *Journal of Materials Chemistry* **2006,** *16* (7), 626-636.
35. Feng, Y.; Chen, Q.; Jiang, M.; Yao, J., Tailoring the properties of UiO-66 through defect engineering: A review. *Industrial & Engineering Chemistry Research* **2019,** *58* (38), 17646-17659.
36. Qiu, J.; Zhang, X.; Xie, K.; Zhang, X.-F.; Feng, Y.; Jia, M.; Yao, J., Noble metal nanoparticle-functionalized Zr-metal organic frameworks with excellent photocatalytic performance. *Journal of colloid and interface science* **2019,** *538*, 569-577.
37. Qiu, S.; Xue, M.; Zhu, G., Metal–organic framework membranes: from synthesis to separation application. *Chemical Society Reviews* **2014,** *43* (16), 6116-6140.
38. Radwan, A.; Jin, H.; He, D.; Mu, S., Design engineering, synthesis protocols, and energy applications of MOF-derived electrocatalysts. *Nano-Micro Letters* **2021,** *13*, 1-32.
39. Li, B.; Wen, H.-M.; Zhou, W.; Chen, B., Porous metal–organic frameworks for gas storage and separation: what, how, and why? *The journal of physical chemistry letters* **2014,** *5* (20), 3468-3479.

40. Zhang, Z.; Yang, Q.; Cui, X.; Yang, L.; Bao, Z.; Ren, Q.; Xing, H., Sorting of C4 olefins with interpenetrated hybrid ultramicroporous materials by combining molecular recognition and size-sieving. *Angewandte Chemie International Edition* **2017,** *56* (51), 16282-16287.
41. Furukawa, H.; Ko, N.; Go, Y. B.; Aratani, N.; Choi, S. B.; Choi, E.; Yazaydin, A. Ö.; Snurr, R. Q.; O'Keeffe, M.; Kim, J., Ultrahigh porosity in metal-organic frameworks. *Science* **2010,** *329* (5990), 424-428.
42. Ahmadijokani, F.; Molavi, H.; Rezakazemi, M.; Tajahmadi, S.; Bahi, A.; Ko, F.; Aminabhavi, T. M.; Li, J.-R.; Arjmand, M., UiO-66 metal–organic frameworks in water treatment: A critical review. *Progress in Materials Science* **2022,** *125*, 100904.
43. Mason, J. A.; Sumida, K.; Herm, Z. R.; Krishna, R.; Long, J. R., Evaluating metal–organic frameworks for post-combustion carbon dioxide capture via temperature swing adsorption. *Energy & Environmental Science* **2011,** *4* (8), 3030-3040.
44. He, Y.; Zhou, W.; Qian, G.; Chen, B., Methane storage in metal–organic frameworks. *Chemical Society Reviews* **2014,** *43* (16), 5657-5678.
45. Gómez-Gualdrón, D. A.; Colón, Y. J.; Zhang, X.; Wang, T. C.; Chen, Y.-S.; Hupp, J. T.; Yildirim, T.; Farha, O. K.; Zhang, J.; Snurr, R. Q., Evaluating topologically diverse metal–organic frameworks for cryo-adsorbed hydrogen storage. *Energy & Environmental Science* **2016,** *9* (10), 3279-3289.
46. He, Y.; Chen, F.; Li, B.; Qian, G.; Zhou, W.; Chen, B., Porous metal–organic frameworks for fuel storage. *Coordination Chemistry Reviews* **2018,** *373*, 167-198.
47. McDonald, T. M.; Lee, W. R.; Mason, J. A.; Wiers, B. M.; Hong, C. S.; Long, J. R., Capture of carbon dioxide from air and flue gas in the alkylamine-appended metal–organic framework mmen-Mg2 (dobpdc). *Journal of the American Chemical Society* **2012,** *134* (16), 7056-7065.
48. Li, J.; Bhatt, P. M.; Li, J.; Eddaoudi, M.; Liu, Y., Recent progress on microfine design of metal–organic frameworks: structure regulation and gas sorption and separation. *Advanced Materials* **2020,** *32* (44), 2002563.
49. Gonçalves, J. M.; Martins, P. R.; Rocha, D. P.; Matias, T. A.; Juliao, M. S.; Munoz, R. A.; Angnes, L., Recent trends and perspectives in electrochemical sensors based on MOF-derived materials. *Journal of Materials Chemistry C* **2021,** *9* (28), 8718-8745.
50. Ghosh, S. K., *Metal-organic frameworks (MOFs) for environmental applications*. Elsevier: 2019.
51. Venkatasubramanian, A.; Lee, J.-H.; Houk, R. J.; Allendorf, M. D.; Nair, S.; Hesketh, P. J., Characterization of HKUST-1 crystals and their application to MEMS microcantilever array sensors. *ECS Transactions* **2010,** *33* (8), 229.

52. Cheng, T.; Hu, J.; Zhou, C.; Wang, Y.; Zhang, M., Luminescent metal-organic frameworks for nitro explosives detection. *Science China Chemistry* **2016,** *59*, 929-947.
53. Banerjee, D.; Hu, Z.; Li, J., Luminescent metal–organic frameworks as explosive sensors. *Dalton transactions* **2014,** *43* (28), 10668-10685.
54. Li, X.; Li, D.; Zhang, Y.; Lv, P.; Feng, Q.; Wei, Q., Encapsulation of enzyme by metal-organic framework for single-enzymatic biofuel cell-based self-powered biosensor. *Nano Energy* **2020,** *68*, 104308.
55. Chuang, C. H.; Kung, C. W., Metal− organic frameworks toward electrochemical sensors: challenges and opportunities. *Electroanalysis* **2020,** *32* (9), 1885-1895.
56. Bedia, J.; Muelas-Ramos, V.; Peñas-Garzón, M.; Gómez-Avilés, A.; Rodriguez, J. J.; Belver, C., Metal–organic frameworks for water purification. In *Nanomaterials for the Detection and Removal of Wastewater Pollutants*, Elsevier: 2020; pp 241-283.
57. Seo, P. W.; Bhadra, B. N.; Ahmed, I.; Khan, N. A.; Jhung, S. H., Adsorptive removal of pharmaceuticals and personal care products from water with functionalized metal-organic frameworks: remarkable adsorbents with hydrogen-bonding abilities. *Scientific reports* **2016,** *6* (1), 1-11.
58. Crini, G.; Lichtfouse, E., Advantages and disadvantages of techniques used for wastewater treatment. *Environmental Chemistry Letters* **2019,** *17*, 145-155.
59. Wang, C.; Liu, X.; Demir, N. K.; Chen, J. P.; Li, K., Applications of water stable metal–organic frameworks. *Chemical Society Reviews* **2016,** *45* (18), 5107-5134.
60. Rojas, S.; Horcajada, P., Metal–organic frameworks for the removal of emerging organic contaminants in water. *Chemical reviews* **2020,** *120* (16), 8378-8415.
61. Zhang, S.; Wang, J.; Zhang, Y.; Ma, J.; Huang, L.; Yu, S.; Chen, L.; Song, G.; Qiu, M.; Wang, X., Applications of water-stable metal-organic frameworks in the removal of water pollutants: A review. *Environmental Pollution* **2021,** *291*, 118076.
62. Furukawa, H.; Gandara, F.; Zhang, Y.-B.; Jiang, J.; Queen, W. L.; Hudson, M. R.; Yaghi, O. M., Water adsorption in porous metal–organic frameworks and related materials. *Journal of the American Chemical Society* **2014,** *136* (11), 4369-4381.
63. He, J.; Yang, X.; Men, B.; Wang, D., Interfacial mechanisms of heterogeneous Fenton reactions catalyzed by iron-based materials: A review. *Journal of environmental sciences* **2016,** *39*, 97-109.
64. Wang, J. L.; Xu, L. J., Advanced oxidation processes for wastewater treatment: formation of hydroxyl radical and application. *Critical reviews in environmental science and technology* **2012,** *42* (3), 251-325.

65. Chatterjee, D.; Dasgupta, S., Visible light induced photocatalytic degradation of organic pollutants. *Journal of Photochemistry and Photobiology C: Photochemistry Reviews* **2005,** *6* (2-3), 186-205.
66. Chong, M. N.; Jin, B.; Chow, C. W.; Saint, C., Recent developments in photocatalytic water treatment technology: a review. *Water research* **2010,** *44* (10), 2997-3027.
67. Li, W., Metal–organic framework membranes: Production, modification, and applications. *Progress in Materials Science* **2019,** *100*, 21-63.
68. Denny, M. S.; Moreton, J. C.; Benz, L.; Cohen, S. M., Metal–organic frameworks for membrane-based separations. *Nature Reviews Materials* **2016,** *1* (12), 1-17.
69. Wang, X., *Emerging Nanomaterials for Recovery of Toxic and Radioactive Metal Ions from Environmental Media*. Elsevier: 2021.
70. Rochelle, G. T., Amine scrubbing for CO2 capture. *Science* **2009,** *325* (5948), 1652-1654.
71. Liang, Z.; Fu, K.; Idem, R.; Tontiwachwuthikul, P., Review on current advances, future challenges and consideration issues for post-combustion CO2 capture using amine-based absorbents. *Chinese journal of chemical engineering* **2016,** *24* (2), 278-288.
72. Loiseau, T.; Lecroq, L.; Volkringer, C.; Marrot, J.; Férey, G.; Haouas, M.; Taulelle, F.; Bourrelly, S.; Llewellyn, P. L.; Latroche, M., MIL-96, a porous aluminum trimesate 3D structure constructed from a hexagonal network of 18-membered rings and μ 3-oxo-centered trinuclear units. *Journal of the American Chemical Society* **2006,** *128* (31), 10223-10230.
73. Xue, M.; Ma, S.; Jin, Z.; Schaffino, R. M.; Zhu, G.-S.; Lobkovsky, E. B.; Qiu, S.-L.; Chen, B., Robust metal− organic framework enforced by triple-framework interpenetration exhibiting high H2 storage density. *Inorganic chemistry* **2008,** *47* (15), 6825-6828.
74. Britt, D.; Furukawa, H.; Wang, B.; Glover, T. G.; Yaghi, O. M., Highly efficient separation of carbon dioxide by a metal-organic framework replete with open metal sites. *Proceedings of the National Academy of Sciences* **2009,** *106* (49), 20637-20640.
75. Han, S. S.; Jung, D.-H.; Heo, J., Interpenetration of metal organic frameworks for carbon dioxide capture and hydrogen purification: Good or bad? *The Journal of Physical Chemistry C* **2013,** *117* (1), 71-77.
76. Singh Dhankhar, S.; Sharma, N.; Kumar, S.; Dhilip Kumar, T.; Nagaraja, C., Rational Design of a Bifunctional, Two-Fold Interpenetrated ZnII-Metal–Organic Framework for Selective Adsorption of CO2 and Efficient Aqueous Phase Sensing of 2, 4, 6-Trinitrophenol. *Chemistry–A European Journal* **2017,** *23* (64), 16204-16212.

77. Zheng, B.; Bai, J.; Duan, J.; Wojtas, L.; Zaworotko, M. J., Enhanced CO2 binding affinity of a high-uptake rht-type metal− organic framework decorated with acylamide groups. *Journal of the American Chemical Society* **2011,** *133* (4), 748-751.
78. Aniruddha, R.; Sreedhar, I.; Reddy, B. M., MOFs in carbon capture-past, present and future. *Journal of CO2 Utilization* **2020,** *42*, 101297.
79. Younas, M.; Rezakazemi, M.; Daud, M.; Wazir, M. B.; Ahmad, S.; Ullah, N.; Ramakrishna, S., Recent progress and remaining challenges in post-combustion CO2 capture using metal-organic frameworks (MOFs). *Progress in Energy and Combustion Science* **2020,** *80*, 100849.
80. Khalilpour, R.; Mumford, K.; Zhai, H.; Abbas, A.; Stevens, G.; Rubin, E. S., Membrane-based carbon capture from flue gas: a review. *Journal of Cleaner Production* **2015,** *103*, 286-300.
81. Wang, X.; Song, C., Carbon capture from flue gas and the atmosphere: A perspective. *Frontiers in Energy Research* **2020,** *8*, 560849.
82. Yu, C.-H.; Huang, C.-H.; Tan, C.-S., A review of CO2 capture by absorption and adsorption. *Aerosol and Air Quality Research* **2012,** *12* (5), 745-769.
83. Ding, M.; Flaig, R. W.; Jiang, H.-L.; Yaghi, O. M., Carbon capture and conversion using metal–organic frameworks and MOF-based materials. *Chemical Society Reviews* **2019,** *48* (10), 2783-2828.
84. Bavykina, A.; Kolobov, N.; Khan, I. S.; Bau, J. A.; Ramirez, A.; Gascon, J., Metal–organic frameworks in heterogeneous catalysis: recent progress, new trends, and future perspectives. *Chemical reviews* **2020,** *120* (16), 8468-8535.
85. Zhai, Z.; Yan, W.; Dong, L.; Deng, S.; Wilkinson, D. P.; Wang, X.; Zhang, L.; Zhang, J., Catalytically active sites of MOF-derived electrocatalysts: Synthesis, characterization, theoretical calculations, and functional mechanisms. *Journal of Materials Chemistry A* **2021,** *9* (36), 20320-20344.
86. Kökçam-Demir, Ü.; Goldman, A.; Esrafili, L.; Gharib, M.; Morsali, A.; Weingart, O.; Janiak, C., Coordinatively unsaturated metal sites (open metal sites) in metal–organic frameworks: design and applications. *Chemical Society Reviews* **2020,** *49* (9), 2751-2798.
87. Klet, R. C.; Liu, Y.; Wang, T. C.; Hupp, J. T.; Farha, O. K., Evaluation of Brønsted acidity and proton topology in Zr-and Hf-based metal–organic frameworks using potentiometric acid–base titration. *Journal of Materials Chemistry A* **2016,** *4* (4), 1479-1485.
88. Jiang, J.; Yaghi, O. M., Brønsted acidity in metal–organic frameworks. *Chemical reviews* **2015,** *115* (14), 6966-6997.

89. Lawrence, A. S.; Sivakumar, B.; Dhakshinamoorthy, A., Detecting Lewis acid sites in metal-organic frameworks by density functional theory. *Molecular Catalysis* **2022,** *517*, 112042.
90. Liu, M.; Wu, J.; Hou, H., Metal–Organic Framework (MOF)-based materials as heterogeneous catalysts for C− H bond activation. *Chemistry–A European Journal* **2019,** *25* (12), 2935-2948.
91. Luo, R.; Yang, Y.; Chen, K.; Liu, X.; Chen, M.; Xu, W.; Liu, B.; Ji, H.; Fang, Y., Tailored covalent organic frameworks for simultaneously capturing and converting CO 2 into cyclic carbonates. *Journal of Materials Chemistry A* **2021,** *9* (37), 20941-20956.
92. Razavi, S. A. A.; Morsali, A., Linker functionalized metal-organic frameworks. *Coordination Chemistry Reviews* **2019,** *399*, 213023.
93. Mandal, S.; Natarajan, S.; Mani, P.; Pankajakshan, A., Post-synthetic modification of metal–organic frameworks toward applications. *Advanced Functional Materials* **2021,** *31* (4), 2006291.
94. Shu, Y.; Ye, Q.; Dai, T.; Xu, Q.; Hu, X., Encapsulation of luminescent guests to construct luminescent metal–organic frameworks for chemical sensing. *ACS sensors* **2021,** *6* (3), 641-658.
95. Cui, Y.; Li, B.; He, H.; Zhou, W.; Chen, B.; Qian, G., Metal–organic frameworks as platforms for functional materials. *Accounts of chemical research* **2016,** *49* (3), 483-493.
96. Jiao, L.; Jiang, H.-L., Metal-organic frameworks for catalysis: Fundamentals and future prospects. *Chinese Journal of Catalysis* **2023,** *45*, 1-5.
97. Adatoz, E.; Avci, A. K.; Keskin, S., Opportunities and challenges of MOF-based membranes in gas separations. *Separation and Purification Technology* **2015,** *152*, 207-237.
98. Chueh, C.-C.; Chen, C.-I.; Su, Y.-A.; Konnerth, H.; Gu, Y.-J.; Kung, C.-W.; Wu, K. C.-W., Harnessing MOF materials in photovoltaic devices: recent advances, challenges, and perspectives. *Journal of Materials Chemistry A* **2019,** *7* (29), 17079-17095.
99. Peng, Y.; Zhou, T.; Ma, J.; Bai, Y.; Cao, S.; Pang, H., Metal-organic framework (MOF) composites as promising materials for energy storage applications. *Advances in Colloid and Interface Science* **2022**, 102732.
100. Liu, C.; Wang, J.; Wan, J.; Yu, C., MOF-on-MOF hybrids: Synthesis and applications. *Coordination Chemistry Reviews* **2021,** *432*, 213743.
101. Chui, S. S.-Y.; Lo, S. M.-F.; Charmant, J. P.; Orpen, A. G.; Williams, I. D., A chemically functionalizable nanoporous material [Cu3 (TMA) 2 (H2O) 3] n. *Science* **1999,** *283* (5405), 1148-1150.
102. Li, H.; Eddaoudi, M.; O'Keeffe, M.; Yaghi, O. M., Design and synthesis of an exceptionally stable and highly porous metal-organic framework. *nature* **1999,** *402* (6759), 276-279.

103. Cavka, J. H.; Jakobsen, S.; Olsbye, U.; Guillou, N.; Lamberti, C.; Bordiga, S.; Lillerud, K. P., A new zirconium inorganic building brick forming metal organic frameworks with exceptional stability. *Journal of the American Chemical Society* **2008,** *130* (42), 13850-13851.
104. Wu, H.; Chua, Y. S.; Krungleviciute, V.; Tyagi, M.; Chen, P.; Yildirim, T.; Zhou, W., Unusual and highly tunable missing-linker defects in zirconium metal–organic framework UiO-66 and their important effects on gas adsorption. *Journal of the American Chemical Society* **2013,** *135* (28), 10525-10532.
105. Vandichel, M.; Hajek, J.; Ghysels, A.; De Vos, A.; Waroquier, M.; Van Speybroeck, V., Water coordination and dehydration processes in defective UiO-66 type metal organic frameworks. *CrystEngComm* **2016,** *18* (37), 7056-7069.
106. Trickett, C. A.; Gagnon, K. J.; Lee, S.; Gándara, F.; Bürgi, H. B.; Yaghi, O. M., Definitive molecular level characterization of defects in UiO-66 crystals. *Angewandte Chemie International Edition* **2015,** *54* (38), 11162-11167.
107. Zheng, H.-Q.; Zeng, Y.-N.; Chen, J.; Lin, R.-G.; Zhuang, W.-E.; Cao, R.; Lin, Z.-J., Zr-based metal–organic frameworks with intrinsic peroxidase-like activity for ultradeep oxidative desulfurization: mechanism of H2O2 decomposition. *Inorganic Chemistry* **2019,** *58* (10), 6983-6992.
108. Mondloch, J. E.; Katz, M. J.; Planas, N.; Semrouni, D.; Gagliardi, L.; Hupp, J. T.; Farha, O. K., Are Zr 6-based MOFs water stable? Linker hydrolysis vs. capillary-force-driven channel collapse. *Chemical communications* **2014,** *50* (64), 8944-8946.
109. Yang, D.; Ortuño, M. A.; Bernales, V.; Cramer, C. J.; Gagliardi, L.; Gates, B. C., Structure and dynamics of Zr6O8 metal–organic framework node surfaces probed with ethanol dehydration as a catalytic test reaction. *Journal of the American Chemical Society* **2018,** *140* (10), 3751-3759.
110. Shearer, G. C.; Chavan, S.; Bordiga, S.; Svelle, S.; Olsbye, U.; Lillerud, K. P., Defect engineering: tuning the porosity and composition of the metal–organic framework UiO-66 via modulated synthesis. *Chemistry of Materials* **2016,** *28* (11), 3749-3761.
111. Yuan, S.; Feng, L.; Wang, K.; Pang, J.; Bosch, M.; Lollar, C.; Sun, Y.; Qin, J.; Yang, X.; Zhang, P., Stable metal–organic frameworks: design, synthesis, and applications. *Advanced Materials* **2018,** *30* (37), 1704303.
112. Lam, E.; Larmier, K.; Wolf, P.; Tada, S.; Safonova, O. V.; Copéret, C., Isolated Zr surface sites on silica promote hydrogenation of CO2 to CH3OH in supported Cu catalysts. *Journal of the American Chemical Society* **2018,** *140* (33), 10530-10535.
113. Larmier, K.; Liao, W. C.; Tada, S.; Lam, E.; Verel, R.; Bansode, A.; Urakawa, A.; Comas-Vives, A.; Copéret, C., CO2-to-methanol

hydrogenation on zirconia-supported copper nanoparticles: reaction intermediates and the role of the metal–support interface. *Angewandte Chemie International Edition* **2017,** *56* (9), 2318-2323.
114. Lam, E.; Larmier, K.; Tada, S.; Wolf, P.; Safonova, O. V.; Copéret, C., Zr (IV) surface sites determine CH3OH formation rate on Cu/ZrO2/SiO2-CO2 hydrogenation catalysts. *Chinese Journal of Catalysis* **2019,** *40* (11), 1741-1748.
115. Lam, E.; Corral-Pérez, J. J.; Larmier, K.; Noh, G.; Wolf, P.; Comas-Vives, A.; Urakawa, A.; Copéret, C., CO2 hydrogenation on Cu/Al2O3: role of the metal/support interface in driving activity and selectivity of a bifunctional catalyst. *Angewandte Chemie International Edition* **2019,** *58* (39), 13989-13996.
116. Rungtaweevoranit, B.; Baek, J.; Araujo, J. R.; Archanjo, B. S.; Choi, K. M.; Yaghi, O. M.; Somorjai, G. A., Copper nanocrystals encapsulated in Zr-based metal–organic frameworks for highly selective CO2 hydrogenation to methanol. *Nano letters* **2016,** *16* (12), 7645-7649.
117. An, B.; Zhang, J.; Cheng, K.; Ji, P.; Wang, C.; Lin, W., Confinement of ultrasmall cu/zno x nanoparticles in metal–organic frameworks for selective methanol synthesis from catalytic hydrogenation of co2. *Journal of the American Chemical Society* **2017,** *139* (10), 3834-3840.
118. Román-Martínez, M.; Cazorla-Amorós, D.; Salinas-Martínez de Lecea, C.; Linares-Solano, A., Structure sensitivity of CO2 hydrogenation reaction catalyzed by Pt/carbon catalysts. *Langmuir* **1996,** *12* (2), 379-385.
119. Wei, J.; Iglesia, E., Mechanism and site requirements for activation and chemical conversion of methane on supported Pt clusters and turnover rate comparisons among noble metals. *The Journal of Physical Chemistry B* **2004,** *108* (13), 4094-4103.
120. Gutterød, E. S.; Pulumati, S. H.; Kaur, G.; Lazzarini, A.; Solemsli, B. G.; Gunnæs, A. E.; Ahoba-Sam, C.; Kalyva, M. E.; Sannes, J. A.; Svelle, S.; Skúlason, E.; Nova, A.; Olsbye, U., Influence of Defects and H2O on the Hydrogenation of CO2 to Methanol over Pt Nanoparticles in UiO-67 Metal–Organic Framework. *Journal of the American Chemical Society* **2020,** *142* (40), 17105-17118.
121. Gutterød, E. S.; Lazzarini, A.; Fjermestad, T.; Kaur, G.; Manzoli, M.; Bordiga, S.; Svelle, S.; Lillerud, K. P.; Skúlason, E.; Øien-Ødegaard, S., Hydrogenation of CO2 to methanol by Pt nanoparticles encapsulated in UiO-67: deciphering the role of the metal–organic framework. *Journal of the American Chemical Society* **2019,** *142* (2), 999-1009.
122. Schrödinger, E., An undulatory theory of the mechanics of atoms and molecules. *Physical review* **1926,** *28* (6), 1049.
123. Griffiths, D. J.; Schroeter, D. F., *Introduction to quantum mechanics*. Cambridge university press: 2018.

124. Born, M.; Heisenberg, W., Zur quantentheorie der molekeln. *Original Scientific Papers Wissenschaftliche Originalarbeiten* **1985**, 216-246.
125. Hartree, D. R. In *The wave mechanics of an atom with a non-Coulomb central field. Part I. Theory and methods*, Mathematical Proceedings of the Cambridge Philosophical Society, Cambridge university press: 1928; pp 89-110.
126. Slater, J. C., The theory of complex spectra. *Physical Review* **1929,** *34* (10), 1293.
127. Fock, V., Näherungsmethode zur Lösung des quantenmechanischen Mehrkörperproblems. *Zeitschrift für Physik* **1930,** *61*, 126-148.
128. Maurice, D.; Head-Gordon, M., Analytical second derivatives for excited electronic states using the single excitation configuration interaction method: theory and application to benzo [a] pyrene and chalcone. *Molecular Physics* **1999,** *96* (10), 1533-1541.
129. Head-Gordon, M.; Maurice, D.; Oumi, M., A perturbative correction to restricted open shell configuration interaction with single substitutions for excited states of radicals. *Chemical physics letters* **1995,** *246* (1-2), 114-121.
130. Purvis III, G. D.; Bartlett, R. J., A full coupled-cluster singles and doubles model: The inclusion of disconnected triples. *The Journal of Chemical Physics* **1982,** *76* (4), 1910-1918.
131. Thomas, L. H. In *The calculation of atomic fields*, Mathematical proceedings of the Cambridge philosophical society, Cambridge University Press: 1927; pp 542-548.
132. Hohenberg, P.; Kohn, W., Inhomogeneous electron gas. *Physical review* **1964,** *136* (3B), B864.
133. Bagayoko, D., Understanding density functional theory (DFT) and completing it in practice. *AIP Advances* **2014,** *4* (12).
134. Cottenier, S., Density Functional Theory and the family of (L) APW-methods: a step-by-step introduction. *Instituut voor Kern-en Stralingsfysica, KU Leuven, Belgium* **2002,** *4* (0), 41.
135. Kohn, W.; Sham, L. J., Self-consistent equations including exchange and correlation effects. *Physical review* **1965,** *140* (4A), A1133.
136. Vosko, S.; Wilk, L., Influence of an improved local-spin-density correlation-energy functional on the cohesive energy of alkali metals. *Physical Review B* **1980,** *22* (8), 3812.
137. Dirac, P. A. In *Note on exchange phenomena in the Thomas atom*, Mathematical proceedings of the Cambridge philosophical society, Cambridge University Press: 1930; pp 376-385.
138. Burke, K.; Wagner, L. O., DFT in a nutshell. *International Journal of Quantum Chemistry* **2013,** *113* (2), 96-101.
139. Perdew, J. P.; Chevary, J. A.; Vosko, S. H.; Jackson, K. A.; Pederson, M. R.; Singh, D. J.; Fiolhais, C., Atoms, molecules, solids, and

surfaces: Applications of the generalized gradient approximation for exchange and correlation. *Physical review B* **1992,** *46* (11), 6671.
140. Perdew, J. P.; Burke, K.; Ernzerhof, M., Generalized Gradient Approximation Made Simple. *Physical Review Letters* **1996,** *77* (18), 3865-3868.
141. Becke, A. D., A new mixing of Hartree–Fock and local density-functional theories. *The Journal of chemical physics* **1993,** *98* (2), 1372-1377.
142. Heyd, J.; Scuseria, G. E.; Ernzerhof, M., Hybrid functionals based on a screened Coulomb potential. *The Journal of chemical physics* **2003,** *118* (18), 8207-8215.
143. Stephens, P. J.; Devlin, F. J.; Chabalowski, C. F.; Frisch, M. J., Ab initio calculation of vibrational absorption and circular dichroism spectra using density functional force fields. *The Journal of physical chemistry* **1994,** *98* (45), 11623-11627.
144. Slater, J., Cohesion in Monovalent 1! etals1', Phys. Rev. 35-'509 and. *Atomic Shelding Constantsf1, Phys. Rev* **1930,** *36*, 57.
145. Gill, P., Advances in quantum chemistry. *Yol* **1994,** *25* (25), 141.
146. Boys, S. F., Electronic wave functions-I. A general method of calculation for the stationary states of any molecular system. *Proceedings of the Royal Society of London. Series A. Mathematical and Physical Sciences* **1950,** *200* (1063), 542-554.
147. Bloch, F., Quantum mechanics of electrons in crystal lattices. *Z. Phys* **1928,** *52*, 555-600.
148. Schwerdtfeger, P., The pseudopotential approximation in electronic structure theory. *ChemPhysChem* **2011,** *12* (17), 3143-3155.
149. Hellmann, H., A new approximation method in the problem of many electrons. *The Journal of Chemical Physics* **1935,** *3* (1), 61-61.
150. Kresse, G.; Joubert, D., From ultrasoft pseudopotentials to the projector augmented-wave method. *Physical review b* **1999,** *59* (3), 1758.
151. LIPPERT, B. G.; PARRINELLO, J. H.; MICHELE, A hybrid Gaussian and plane wave density functional scheme. *Molecular Physics* **1997,** *92* (3), 477-488.
152. Dunning Jr, T. H., Gaussian basis sets for use in correlated molecular calculations. I. The atoms boron through neon and hydrogen. *The Journal of chemical physics* **1989,** *90* (2), 1007-1023.
153. Liptrot, D. J.; Power, P. P., London dispersion forces in sterically crowded inorganic and organometallic molecules. *Nature Reviews Chemistry* **2017,** *1* (1), 0004.
154. Grimme, S.; Antony, J.; Ehrlich, S.; Krieg, H., A consistent and accurate ab initio parametrization of density functional dispersion correction (DFT-D) for the 94 elements H-Pu. *The Journal of Chemical Physics* **2010,** *132* (15), 154104.

155. Grimme, S.; Ehrlich, S.; Goerigk, L., Effect of the damping function in dispersion corrected density functional theory. *Journal of Computational Chemistry* **2011,** *32* (7), 1456-1465.
156. Henkelman, G.; Uberuaga, B. P.; Jónsson, H., A climbing image nudged elastic band method for finding saddle points and minimum energy paths. *The Journal of Chemical Physics* **2000,** *113* (22), 9901-9904.
157. Henkelman, G.; Jónsson, H., Improved tangent estimate in the nudged elastic band method for finding minimum energy paths and saddle points. *The Journal of Chemical Physics* **2000,** *113* (22), 9978-9985.

Included Publications

Paper I

Paper II